SRNL-STI-2009-00149, Revision 0

Keywords: DWPF, melter, mercury, oxidation model

Retention: Permanent

Modeling the Impact of Elevated Mercury in Defense Waste Processing Facility Melter Feed on the Melter Off-Gas System – Preliminary Report

J. R. Zamecnik
A. S. Choi

March 2009

Savannah River National Laboratory
Savannah River Nuclear Solutions
Aiken, SC 29808

Prepared for the U.S. Department of Energy under Contract No. DE-AC09-08SR22470

DISCLAIMER

Printed in the United States of America

Prepared for the
U.S. Department of Energy

SRNL-STI-2009-00149, Revision 0

Keywords: DWPF, melter, mercury, oxidation model

Retention: Permanent

Modeling the Impact of Elevated Mercury in Defense Waste Processing Facility Melter Feed on the Melter Off-Gas System – Preliminary Report

J. R. Zamecnik
A. S. Choi

March 2009

Savannah River National Laboratory
Savannah River Nuclear Solutions
Aiken, SC 29808

Prepared for the U.S. Department of Energy under Contract No. DE-AC09-08SR22470

REVIEWS AND APPROVALS

AUTHORS:

J.R. Zamecnik, Engineering Process Development Date

A.S. Choi, Engineering Process Development Date

D.C. Koopman, Peer Reviewer, Process Engineering Technology Date

A.B. Barnes, Manager, Engineering Process Development Date

S.L. Marra, Manager, Date
Environmental & Chemical Process Technology Research Programs

J.E. Occhipinti, Manager, WSRC Waste Solidification Engineering Date

TABLE OF CONTENTS

LIST OF FIGURES

LIST OF TABLES

LIST OF ACRONYMS & ABBREVIATIONS

(aq)	aqueous
(ℓ)	liquid
(s)	solid
(v)	vapor
CPC	Chemical Processing Cell
DWPF	Defense Waste Processing Facility
EDS	energy-dispersive spectroscopy
EPA	Environmental Protection Agency
ESCM	Experimental Scale Ceramic Melter
HEME	high efficiency mist eliminator
HEPA	high efficiency particulate air
IDMS	Integrated DWPF Melter System
K	equilibrium constant
k	rate constant
L	liter
LP/LIF	laser photolysis/laser induced fluorescence
m	molal, mol/kg solvent
M	molar, mol/L
mM	millimolar
mmol	millimol
ms	millisecond
NA	not available
ND	none detected
NM	not measured
OGC	off-gas condenser
OGCT	off-gas condensate tank
OLI	OLI Systems, Inc. – aqueous simulation software publisher
PNNL	Pacific Northwest National Laboratory
ppbv	parts per billion by volume (or mol)
ppm	parts per million = mg/L herein
redox	reduction-oxidation
s	second
SAS	steam-atomized scrubber
SB5	sludge batch 5
SEM	scanning electron microscopy
SRAT	sludge receipt and adjustment tank
SRNL	Savannah River National Laboratory
TS	total solids (wt%)
VS	vapor space
wt%	weight percent
XRD	x-ray diffraction

1.0 EXECUTIVE SUMMARY

The Defense Waste Processing Facility (DWPF) is currently evaluating an alternative Chemical Process Cell (CPC) flowsheet to increase throughput. It includes removal of the steam-stripping step, which would significantly reduce the CPC processing time and lessen the sampling needs. However, its downside would be to send 100% of the mercury that come in with the sludge straight to the melter. For example, the new mercury content in the Sludge Batch 5 (SB5) melter feed is projected to be 25 times higher than that in the SB4 with nominal steam stripping of mercury. This task was initiated to study the impact of the worst-case scenario of zero-mercury-removal in the CPC on the DWPF melter off-gas system. It is stressed that this study is intended to be scoping in nature, so the results presented in this report are preliminary.

In order to study the impact of elevated mercury levels in the feed, it is necessary to be able to predict how mercury would speciate in the melter exhaust under varying melter operating conditions. A homogeneous gas-phase oxidation model of mercury by chloride was developed to do just that. The model contains two critical parameters pertaining to the partitioning of chloride among HCl, Cl, Cl_2, and chloride salts in the melter vapor space. The values for these parameters were determined at two different melter vapor space temperatures by matching the calculated molar ratio of HgCl (or Hg_2Cl_2) to $HgCl_2$ with those measured during the Experimental-Scale Ceramic Melter (ESCM) tests run at the Pacific Northwest National Laboratory (PNNL).[1]

The calibrated model was then applied to the SB5 simulant used in the earlier flowsheet study[2] with an assumed mercury stripping efficiency of zero; the molar ratio of Cl-to-Hg in the resulting melter feed was only 0.4, compared to 12 for the ESCM feeds. The results of the model run at the indicated melter vapor space temperature of 650 °C (TI4085D) showed that due to excessive shortage of chloride, only 6% of the mercury fed is expected to get oxidized, mostly as HgCl, while the remaining mercury would exist either as elemental mercury vapor (90%) or HgO (4%).

Noting that the measured chloride level in the SB5 qualification sample was an order of magnitude lower than that used in the SB5 simulant, the degree of chloride shortage will be even greater. As a result, the projected level of HgCl in the actual SB5 melter exhaust will be even lower than 6% of the total mercury fed, while that of elemental mercury is likely to be greater than 90%.

The homogeneous oxidation of mercury in the off-gas was deemed to be of primary importance based on the postulation that mercury and other volatile salts form sub-micron sized aerosols upon condensation and thus remain largely in the gas stream downstream of the quencher where they can deposit in the off-gas lines, Steam-Atomized Scrubbers (SAS), and High-Efficiency Mist Eliminator (HEME). Formation of these sub-micron semi-volatile salts in the condensate liquid is considered to be unlikely, so the liquid phase reactions were considered to be less important. However, subsequent oxidation of mercury in the liquid phase in the off-gas system was examined in a

simplified model of the off-gas condensate. It was found that the condensate chemistry was consistent with further oxidation of elemental mercury to Hg_2Cl_2 and conversion of HgO to chlorides. The results were consistent with the available experimental data.

It should also be noted that the model predictions presented in this report do not include any physically entrained solids, which typically account for much of the off-gas carryover on a mass basis. The high elemental mercury vapor content predicted at the DWPF Quencher inlet means that physically entrained solids could provide the necessary surface onto which elemental mercury vapor could condense, thereby coating the solids as well as the internal surfaces of the off-gas system with mercury.

Clearly, there are many process benefits to be gained by removing the steam-stripping step from the CPC cycle. The goal of this task was to study what adverse impact the zero-mercury-removal scenario would have on the DWPF melter off-gas system operation. It is stressed again that this study was intended to be scoping in nature, so the results presented in this report are preliminary. Any further substantiation of these results for actual implementation into the DWPF flowsheet would require an in-depth modeling study of all three reaction zones, including the aqueous-phase reactions in the quencher, OGCT, Steam Atomized Scrubber (SAS), and off-gas condenser with recirculated condensate, and the proof-of-principle experiments.

2.0 INTRODUCTION

The Savannah River National Laboratory (SRNL) was requested to review pertinent literature on mercury behavior in off-gas systems and then to perform flowsheet material balances on the DWPF melter off-gas stream to determine the feasibility of removing all mercury from the OGCT.[3] This request was part of a larger request to assess the feasibility of using an alternative to formic acid as the reductant for the melter feed. It is expected that this alternative reductant will not convert mercuric oxide (HgO) in the sludge feed to elemental Hg (Hg°), which can be steam stripped from the waste in the Sludge Receipt and Adjustment Tank (SRAT). In this off-gas feasibility determination, the effect of the chosen reductant on the melter off-gas mercury is assumed to be negligible as mercury is emitted from the melter entirely as Hg°.

DWPF Sludge Batches 1-4 contained low levels of mercury such that the SRAT product typically met the design basis requirement of less than 0.45 wt% Hg in the total solids. Operation without mercury removal for SB5 would push the mercury concentration up to 2 wt% of the SRAT product solids so that the mercury content in the SB5 melter feed would be more than 25 times higher than that of SB4 with nominal mercury removal. The concern is the potential impact that these elevated mercury levels would have on the operation of the DWPF melter and off-gas system. In order to address this concern, it is necessary to know how mercury would speciate throughout the melter off-gas system under different operating conditions. It is precisely the goal of this study to determine the off-gas chemistry of mercury through a thorough literature survey and some scoping model simulations.

2.1 MERCURY MEASUREMENT IN MELTER OFF-GAS

2.1.1 DWPF Melter Off-Gas Deposits and OGCT Liquid

The nominal amounts of Hg and Cl in the incoming DWPF sludge batches (SB) and their SRAT products are shown in Table 2-1. The molar Cl/Hg ratio in the melter feed should equal the SRAT product ratio. For SB1A and SB3, there was excess Cl, while for SB2, SB4, and SB5 there has been excess Hg. The proposed operation without Hg stripping with SB5 would give the lowest Cl/Hg ratio yet used. Note that the SB5 simulant chloride is significantly higher than the other values, due to using $RuCl_3$ as the Ru source.

Table 2-1 Average Mercury in SRAT Feed & SRAT Product (after Hg Stripping)

----------mmol/kg of slurry----------

Sample	Feed Total Hg	Feed Total Cl	SRAT Product Total Hg	SRAT Product Total Cl	SRAT Product Cl/Hg
Sludge Batch 1A	1.42	0.92	<0.50	1.08	>2.2
Sludge Batch 1B	10.1	NA	<0.50	NA	NA
Sludge Batch 2	1.79	0.35	<0.50	0.39	>0.78
Sludge Batch 3	1.36	0.64	<0.50	0.81	>1.6
Sludge Batch 4	5.86	0.66	1.71	0.94	0.55
Sludge Batch 5[1]	12.1	0.56	3.22	0.81	0.25
Sludge Batch 5[2] No Stripping	16.7	0.56	16.7	0.56	0.034
Sludge Batch 5 Simulant	16.7	8.59	16.7	0.56	0.51

[1] SB5 Qualification sample [2] SB5 possible high concentration

Samples of solid deposits in the DWPF melter off-gas system were taken and analyzed in 2003[4] and 2007.[5] An OGCT sample was analyzed in 2004.[6] In a 2005 analysis of the OGCT, mercury concentration was not measured.[7] The mercury and chloride analyses of these samples are summarized in Table 2-2. Total chloride was not measured in any of the samples; soluble mercury was measured only for the Steam Atomized Scrubber (SAS) deposits. X-ray diffraction (XRD) and SEM-EDS of the 2003 samples did not indicate the presence of any Hg species; XRD would only find crystalline species at greater than ~0.5 wt% and SEM-EDS could find both crystalline and amorphous species at about the same concentration. Calomel, Hg_2Cl_2, was found to be the predominant Hg species and it also constituted a significant portion of the SAS inlet samples from 2007. Qualitatively, the SAS deposits were grayer than the quencher deposits, consistent with the presence of calomel, which disproportionates slightly to Hg^0 (grayish) and $HgCl_2$.

The soluble Hg content of the SAS inlet samples indicates that soluble Hg was about 6-10% of the total mercury. Soluble Hg is expected to be $HgCl_2$, because $HgCl_2$ is the only likely mercury compound to have significant solubility (~0.26 mol/kg water @ 25°C).[8,9] Hg_2Cl_2 has an extremely low solubility (K_{sp} = 1.42 x 10^{-18} mol^3 kg^{-3} @ 25°C);[10] it is actually more likely to disproportionate into Hg^0 and $HgCl_2$:[11]

$$Hg_2Cl_2(s) = Hg^0(\ell) + HgCl_2(aq) \qquad K = 2.35 \times 10^{-7} \text{ mol kg}^{-1}$$

On a molar basis, the total Hg in the 2007 quencher inlet sample was 6.0-7.5 mmol/kg. Assuming this Hg was present as Hg_2Cl_2, there would be an equal number of moles of Cl in the solids that were not measured because the Hg_2Cl_2 would not have dissolved. Adding this Cl to the measured soluble Cl (5.6 mmol/kg) gives the estimated total Cl values. For the quencher inlet, the estimated total Cl was about twice the total Hg; for the SAS inlet, there was relatively less soluble Cl. The OGCT liquid samples from 2004 showed significantly less soluble Cl relative to the total Hg, which suggests that about 95% of the Cl was in Hg_2Cl_2.

Table 2-2 DWPF OGCT and Off-Gas Deposit Mercury and Chloride Concentrations

Concentration (wt% of dried solids)

Sample & Date	Number of Samples	Total Hg (wt% of dried solids)	Soluble Hg* (wt% of dried solids)	Soluble Cl* (wt% of dried solids)
Film Cooler Exit (2003)	1	ND	NM	<0.02
Quencher Inlet (2003)	3	ND, ND, 0.52	NM	<0.02
Quencher Bottom (2003)	2	ND, 0.77	NM	<0.02
Quencher Inlet (2007)	3	0.12-0.15	NM	0.02
SAS Inlet (2007)	3	3.42-6.57	0.35-0.43	0.20
OGCT Liquid (2004)	1	0.0364	NM	0.0005

(The wt% of dried solids in the liquid sample was 0.44 wt%.)

Concentration (mmol/kg of dried solids)

	Total Hg (mmol/kg)	Estimated Total Cl (mmol/kg)	Soluble Hg* (mmol/kg)	Soluble Cl* (mmol/kg)	Total Cl / Total Hg (mol/mol)
Quencher Inlet (2007)	6.0-7.5	11-13	NM	5.6	~1.78
SAS Inlet (2007)	170-328	226-384	17-21	56	~1.17-1.33
OGCT Liquid (2004)	0.18 (1.6 mg/L)	0.32	NM	0.14 (5 mg/L)	~1.78

* dissolved in warm water leach; NM: not measured; ND: none detected, detection limit not stated

Soluble Hg as $HgCl_2$ would have a Cl:Hg molar ratio of 2.0. This ratio for the quencher and OGCT samples is about 1.78. However, this value would be consistent with mostly $HgCl_2$ but also with a mixture of Hg_2Cl_2 and other soluble chlorides such as NaCl. The much lower Cl/Hg ratio for the SAS inlet samples indicates that the amount of Hg as Hg_2Cl_2 must be significant.

2.1.2 Integrated DWPF Melter System (IDMS) Off-Gas System

Mercury measurements were performed during three runs of the IDMS (Runs Hg1, Hg2, Hg3).[12,13] Mercury concentrations were measured in the melter off-gas to the quencher, OGCT to SAS line, off-gas condenser (OGC) exit, and the high-efficiency mist eliminator (HEME) exit. These measurements were of total Hg and were done by drawing a gas sample through impingers containing acidic potassium permanganate (EPA Method 111). OGCT samples were also analyzed for soluble mercury and total mercury. Soluble mercury was analyzed by standard wastewater methods with cold vapor atomic absorption spectroscopy. Total mercury was analyzed similarly after dissolution of solids in 1:1 HNO_3:HCl. No particulate mercury was found by X-ray fluorescence (XRF) and SEM-EDS of filter paper samples in the Method 111 sampling train; note that the sensitivity of these methods is only about 0.1 wt%, so there could have actually been calomel present.

The concentrations of mercury in the melter feed were extremely low, even though the initial Hg concentration in the simulated sludge was 11 mmol/kg, which is within the range run in DWPF. Values ranged from 6.3 to 37 mg/L compared to a DWPF SB4 value of approximately 170 mg/L. Material balance closure was good (92-122%) using the melter feed and OGCT Hg concentrations; the vapor stream exiting the HEME was negligible compared to these flows. The measured concentrations of total mercury at six

locations are summarized in Table 2-3. The concentration of Cl in these feeds was approximately 1000 mg/L, so the Cl/Hg molar ratio was about 151 to 936, which is much higher than the DWPF values.

Table 2-3 Mercury in IDMS Melter Feed and Off-Gas System

Sample Location	Saturation Temperature (°C)	Run Hg1	Run Hg2	Run Hg3	Hg at Saturation (ppbv)	$HgCl_2$ at Saturation (ppbv)
Melter Feed	NA	6.3 mg/L 0.031 mM	10.8 mg/L 0.054 mM	37.0 mg/L 0.18 mM	NA	NA
Melter Off-gas to Quencher	NA	NM	205 ppbv	1185 ppbv	NA	NA
OGCT Exit to SAS	45-60	NM	19 ppbv	249 ppbv	11400-32500	1120-4750
SAS/OGC Exit	~10	NM	3.6 ppbv	**154 ppbv**	631	21
HEME Exit	~10	NM	1.9 ppbv	**34 ppbv**	631	21
OGCT Liquid (Maximum)	NA	NM	1.9 mg/L	11.9 mg/L	NA	NA

ppbv: parts per billion by volume (or mol); NA: not applicable; NM: not measured

These results show that the concentration of mercury in the melter feed was never high enough to saturate the off-gas in elemental Hg^0 or $HgCl_2$, except at the SAS/OGC exit and HEME exit (bold face) in Hg3. In this run, the total Hg in the vapor exceeds the $HgCl_2$ saturation concentration, so the total Hg *could* have been due to saturated $HgCl_2$ plus Hg^0 at below saturation. The vapor concentrations would depend on the liquid concentrations and Henry's law for dissolved Hg species. If Hg^0 metal were present, it would exert its full vapor pressure.

The maximum amount of Hg in the OGCT was 11.9 mg/L, compared to the only available DWPF analysis of 1.6 mg/L (Table 2-2). Both of these values are significantly lower than the solubilities (25 °C) of Hg^0 in oxygenated water (4200 mg/L), HgO (5200 mg/L), $HgCl_2$ (66000 mg/L), and even Hg_2Cl_2 (200 mg/L), but the IDMS value is higher than the solubility of Hg^0 in un-oxygenated water (~6 mg/L).[14] The high excess Cl in the IDMS runs would be expected to give predominantly $HgCl_2$ in the off-gas condensate.

The percentage the total Hg in OGCT liquid samples that was not dissolved varied from 0-16 wt%. The entrained sludge and glass particles in the condensate were grayish compared to runs without mercury where they were red-brown in color. The gray color indicates the solids were probably coated with elemental mercury metal, which would be counted as undissolved mercury.

2.1.3 Engineering Scale Ceramic Melter (ESCM) at Pacific Northwest Laboratory

The ESCM melter at Pacific Northwest Laboratory was used in 1990 to study mercury speciation in the off-gas system.[1] The off-gas mercury data collected during these tests are the most complete found for glass melter operation. The melter system consisted of a slurry-fed joule-heated melter with a venturi scrubber (quencher), condensate or quench tank (OGCT), chilled-water condenser, and HEPA filter. The feed tested was of a

composition similar to DWPF; the feed was treated with formic acid. Off-gas system tests were conducted at varying plenum temperatures and air inleakage rates. The composition of the Hg, Cl^-, and SO_4^{2-} are shown in Table 2-4 for the ESCM, DWPF, and IDMS melters. Sulfate is shown because of its importance in the redox chemistry of chlorine.

Table 2-4 Melter Feed or SRAT Product Compositions

Melter	Sample	Run	Hg (mM)	Cl^- (mM)	SO_4^{-2} (mM)	Cl^-/Hg	Cl^-/SO_4^{-2}
ESCM	Melter Feed		4.14	49.6	9.78	12.0	5.1
IDMS	Melter Feed	Hg1	0.03	13.7	NA	436	NA
IDMS	Melter Feed	Hg2	0.05	12.9	NA	240	NA
IDMS	Melter Feed	Hg3	0.18	12.4	NA	66.8	NA
DWPF	SRAT Product	SB4	1.98	1.09	12.9	0.55	0.085
DWPF	SRAT Product	SB5	3.68	0.93	5.6	0.25	0.17
DWPF (no Hg removal)	SRAT Product	SB5	18.2	0.62	-	0.034	-

Chlorine was present in the ESCM feed at 12 times the mercury. The IDMS runs also had significant excess chlorine, while DWPF SB4 and SB5 had Cl:Hg ratios of about 0.55 and 0.25, respectively. DWPF SB5, with no mercury removal in the SRAT, would have a Cl:Hg ratio of about 0.034.

Mercury in the vapor was measured in the off-gas directly from the melter off-gas exit, from the two-phase line to the OGCT, at the OGCT exit to the condenser, and after the HEPA. The calculated concentration of Hg at the melter exit was 66-81 ppmv at the 0.73 kg/h air inleakage rate. The melter off-gas exit samples were taken through a particulate filter to a heated sample line and passed through a condenser with liquid trap. The gas then passed through three water-filled impingers before exiting through a pump. The gas-liquid contact in the impingers is somewhat like that in a quencher but not as vigorous. The samples at the other locations were analyzed only for elemental mercury vapor.

For the melter exit samples, no mercury compounds were found on the particulate filters, indicating that no solid Hg_2Cl_2 calomel had been formed. The mercury in the impingers, and also collected in the OGCT liquid, were speciated qualitatively by assuming mercury in the solids was Hg_2Cl_2, while soluble mercury was $HgCl_2$. The identity of the solid mercury species was verified by XRD. The splits of Hg species between Hg_2Cl_2 and $HgCl_2$ for five tests are shown in Table 2-5. The DWPF SAS deposit sample is also shown. No evidence of HgO was found by XRD analysis of samples of the off-gas or condensate.

Table 2-5 ESCM Melter Off-Gas Samples

Test	Air Inleakage (kg/h)	Plenum Temp. (°C)	Impinger Samples (%)		OGCT Samples (%)	
			Hg_2Cl_2	$HgCl_2$	Hg_2Cl_2	$HgCl_2$
1	0.73	750	86	14	89	11
2	6.8	750	38	62	90	10
3	0.73	550	33	67	50	50
4	0.76	740	82	18	NA	NA
5	0.76	740	85	15	NA	NA
DWPF	SAS Deposit	~750	90-94	6-10	-	-

For Tests 1, 4, and 5 (and probably 2) at 750 °C plenum temperature, Hg_2Cl_2 accounted for about 85-90% of the total mercury species found in the impinger samples and the OGCT samples. Test 2 had anomalous results for the impinger samples that did not agree with the OGCT samples; in this test, there is no apparent reason for why the impinger and OGCT sample results would be different. In Test 3 at 550 °C plenum temperature, both the impinger and OGCT samples had significantly more $HgCl_2$ present. Higher plenum temperature appears to favor formation of the less oxidized mercury compound Hg_2Cl_2. The DWPF SAS deposit samples contained about 6-10% soluble Hg ($HgCl_2$), which is consistent with the ESCM results for a 750 °C plenum temperature.

With excess chlorine, the formation of the more oxidized $HgCl_2$ is thermodynamically favored over the formation of Hg_2Cl_2, but Hg_2Cl_2 predominated in most of the tests. The IDMS runs had significantly more excess chlorine and the total mercury concentrations were so low (<12 mg/L Hg) that no Hg_2Cl_2 was ever formed. All of the Hg was probably present as $HgCl_2$. The ESCM tests showed that the concentrations of elemental mercury in the vapor phase at the venturi quencher exit, the OGCT exit, and the condenser/HEPA exit was approximately equal to the saturation vapor pressure at the prevailing temperature. Table 2-6 shows these results.

Table 2-6 ESCM Off-Gas Elemental Mercury Vapor Pressure Temperatures

(Actual is the measured temperature. T_{sat} is the saturation temperature corresponding to the measured mercury partial pressure.)

		Quencher Exit Temperature (°C)		OGCT Exit Temperature (°C)		Condenser/ HEPA Exit Temperature (°C)	
Test	Sample	Actual	T_{sat}	Actual	T_{sat}	Actual	T_{sat}
2	1	40	41		NA		NA
	2	40	41		NA		9
	3	40	35		24		10
	4	41	39		24		11
3	1	32	32	~20	17	~5	6
	2	30	26		18		12
	3	30	27		20		8
	4	30	21		17		11

The measured elemental Hg concentrations at these locations were at saturation even though no elemental mercury metal was ever found in the off-gas system. The authors indicate that the gray color of the calomel was due to Hg^0 on the surface and that it was this small amount of surface Hg^0 exerted its vapor pressure at the different process locations.

Elemental mercury vapor was found in the vapor samples even after melter feeding was discontinued. The authors concluded that the condensate itself was a significant contributor to the elemental mercury concentration in the vapor, and that liquid-vapor equilibrium between the particulate surface elemental mercury and the vapor was approached.

Important Conclusion:

Calomel Hg_2Cl_2 is the primary mercury species in the off-gas system when there is some excess chlorine present. It is the primary species even though $HgCl_2$ is thermodynamically favored in solution when excess chlorine is present.

2.2 GAS PHASE OXIDATION

A large number of papers have been written on the gas phase oxidation of elemental mercury, primarily in coal-fired power plant emissions. In power plants, the mercury and chlorine concentrations in the flue gases are significantly lower than in the melter off-gas systems of interest. Power plant mercury emission levels are typically in the range 0.1 to 4 ppbv (1-30 $\mu g/m^3$)[15] and waste incinerator levels may be up to about 400 ppbv.[16] Mendelsohn and Livengood[17] have reviewed a substantial portion of the literature on mercury chemistry in flue gas. Most papers divide the Hg emissions into insoluble (Hg^0) and soluble ($HgCl_2$), but generally ignore the insoluble Hg_2Cl_2. Generally, the goal for mercury oxidation in power plant flue gases has been oxidation to the soluble $HgCl_2$ that can be scrubbed from the gas. This goal is contrary to that for DWPF where collection of mercury as the insoluble Hg^0 metal might be preferred. The majority of the literature on power plant emissions addresses homogenous reactions of mercury throughout the power plant air pollution control system. A smaller number of papers discuss the possibility of heterogeneous reactions of mercury primarily with the fly ash, but also with the equipment surfaces.

2.2.1 Homogeneous Oxidation

The homogeneous reaction schemes are all similar, but none have been found to be universally applicable to all combustors. For these mechanisms, chlorine atoms (Cl) are assumed to be in excess compared to mercury. The concentration of SO_2 present is usually higher than both Cl and Hg. The primary reaction step in the oxidation is the formation of HgCl from Hg atoms and Cl atoms in the presence of a stabilizing collision partner M:[16,18]

$$Hg + Cl + M \rightarrow HgCl + M \qquad \text{fastest; M is any molecule} \qquad (2.1)$$

The following subsequent reactions are slower:

$$HgCl + HgCl \rightarrow Hg_2Cl_2 \qquad \text{faster} \qquad (2.2)$$
$$HgCl + Cl_2 \rightarrow HgCl_2 + Cl \qquad | \qquad (2.3)$$
$$HgCl + Cl \rightarrow HgCl_2 \qquad \downarrow \qquad (2.4)$$
$$HgCl + HCl \rightarrow HgCl_2 + H \qquad \text{slower} \qquad (2.5)$$

Reaction (2.3) is slow due to the low concentration of Cl_2 present under conditions where there is significant Cl present.

The reactions in Eq. (2.6) are significantly slower in the temperature range where the reactions in (2.2)-(2.5) are significant:

$$\begin{aligned} Hg^0 + Cl_2 &\rightarrow HgCl_2 \\ Hg^0 + HCl &\rightarrow HgCl + H \\ Hg^0 + O_2 &\rightarrow HgO + O \\ Hg^0 + O &\rightarrow HgO \end{aligned} \qquad (2.6)$$

However, some research has suggested homogeneous reactions between Hg and oxygen to form HgO. Hall[19] has suggested a mechanism with HCl and O_2 as important reactants. The reaction of Hg + Cl is limited to the temperature range of about 400-700 °C. Below 400 °C there is too little Cl present to support oxidation, while above 700 °C, atomic Hg^0 is thermodynamically favored. Rate constants for these reactions have been measured or estimated by several groups.[16,18,20,21] Reaction mechanisms with over 100 elementary reaction steps have been proposed.

The rate constant of reaction (2.1) has been found to be mostly independent of temperature. The reaction rate is low at low temperatures because of the lack of Cl radicals. Sliger[16] found that the homogeneous oxidation was primarily governed by the formation of Cl from HCl, the rate at which the hot off-gas was quenched (cooled), and by the presence of background gases involved in competing reactions. These authors also mention the fly ash or carbon mediated reaction where HCl forms Cl_2 that can then react with Hg at temperatures lower than 300 °C. The importance of Cl from Cl_2 has been debated. The formation of Cl_2 from HCl is presumed to be by a metal-catalyzed "Deacon-type" reaction:

$$2\,HCl + \tfrac{1}{2}O_2 \overset{\text{catalyst}}{\rightleftarrows} Cl_2 + H_2O \qquad (2.7)$$

The actual reaction steps for this overall reaction are undoubtedly more complicated, probably involving elementary reactions of H, OH, O, Cl, and other radicals. It is

important to note that when the Cl radical concentration is significant, the molecular chlorine Cl_2 concentration will be relatively small, and vice versa.

Senior[22] suggests that the pathway through HgO may be important in systems with low chlorine concentrations, but Sliger[16] found that no HgO was formed in the absence of HCl in their test gas. Edwards[23] has included oxidation by O_2 in modeling although it apparently has little effect on the overall oxidation rate of Hg. Models by Niksa[24] and Edwards[23] did not predict the oxidation well at less than ~700 °C. Sliger[16] predicted the oxidation was limited to the range 400-700 °C because there were too few Cl radicals at low temperature, while Hg^0 was favored at high temperature. They also noted that virtually all of the oxidation reaction occurred inside their sample probe where cooling at 5400 K/s from about 900 °C occurred. They developed models that showed the extent of Hg oxidation and the equilibrium amount of oxidation during the quench. Complete oxidation was predicted in 60 milliseconds (ms). The kinetically-controlled oxidation extent was only around 40% and was limited by the availability of Cl radicals. Fry[25] has reported that oxidation increased at higher quench rates.

The species NO, NO_2, and SO_2 have been shown to have varying effects on the mercury oxidation rate. Inhibition of oxidation due to the reaction of SO_2 with Cl_2 and H_2O to form HCl and SO_3 has been suggested.[26] Niksa[24] reports that the presence of NO above 100 ppmv limits the oxidation of mercury to negligible levels, but that at high quench rates of >1000 K/s, the presence of NO increases the oxidation rate. They suggested the inhibiting effect of NO was due to the reaction NO + OH + M = HONO + M, which decreased the concentration of the radical OH that is important to Cl radical formation (M is any molecule). Both NO_2 and O_2 have been suggested as important oxidants;[19,27] other work has shown these species to have little effect.[28] In the presence of fly ash, NO_2 was found to increase the oxidation rate, while NO inhibited oxidation in most cases.[29]

2.2.2 Heterogeneous Oxidation

Schofield[30-32] has hypothesized that the main mechanism of mercury oxidation in power plant emissions occurs heterogeneously on the fly ash present and on equipment surfaces. Numerous researchers have reported the difficulty in measuring the rate of homogeneous oxidation due reactions on the surfaces of their test equipment.[16,33-35]

The effect of fly ash on the rate of mercury oxidation was studied for several coals with possible interfering species such as NO_x and SO_2. Laudal[36] has reported that fly ash can have a large effect on speciation. Senior[37] suggests that Cl_2 formed from HCl on the fly ash surface can oxidize Hg. Edwards[23] states that heterogeneous reactions are probably dominant at lower temperature – their model drastically under-predicted mercury oxidation below 630 °C.

The mechanism proposed by Schofield involves the interaction of mercury with surfaces that can accommodate these mercury oxidation reactions. The reactions in Eqs. (2.8) are all surface reactions where the reactive species must first adsorb onto the solid from the vapor phase.

$$\begin{aligned} Hg^0(a) + \tfrac{1}{2}\, O_2 &= HgO(a) \\ Hg^0(a) + SO_2 + O_2 &= HgSO_4(a) \\ HgO(a) + 2\, HCl &= HgCl_2(a) + H_2O \\ HgSO_4(a) + 2\, HCl &= HgCl_2(a) + H_2SO_4 \end{aligned} \qquad (2.8)$$

(a) indicates surface adsorbed species

A mechanism involving only HgO applies when there is no SO_2 present. The actual intermediate on the surface may be H_2SO_4•2HgO. Schofield indicates that mercurous (Hg^{1+}) species are not involved in these surface reactions. Scott[38] has proposed similar surface reactions for reduction of HgO to Hg^0 that also produces HgS from the disproportionation of S(IV) species. These reactions include the formation of a Hg^{1+} sulfate species:

$$\begin{aligned} 2\, HgO\,(a) + SO_2(g) &= Hg^0(a) + HgSO_4(a) \\ Hg^0(a) + HgSO_4(a) &= Hg_2SO_4(a) \\ 2\, Hg^0(a) + 2\, SO_2(g) &= HgS(a) + HgSO_4(a) \end{aligned} \qquad (2.9)$$

2.3 OXIDATION IN AQUEOUS SOLUTIONS

Most of the literature on aqueous oxidation concerns environmental systems such as lakes and rivers. The oxidation of elemental mercury by dissolved oxygen in the presence of chloride anions has been examined by several researchers. Other literature has addressed the unexpected oxidation of Hg^0 in the Ontario Hydro sampling train, which uses a chloride solution to scrub oxidized mercury (Hg^{2+}).[39] The oxidation in this sample train will be briefly discussed as it pertains to the oxidation of mercury in a melter off-gas system.

2.3.1 Oxidation in Dilute Aqueous Solutions

Magalhães[40] studied oxidation of metallic Hg^0 in aqueous solutions containing NaCl. These tests were performed in agitated vessels open to the atmosphere. They found that the oxidation was pseudo zero-order, increasing with temperature up to 25 °C, then remaining constant up to 40 °C. The reaction was monitored by following the concentration of the product $HgCl_4^{2-}$ (Hg^{2+}). $HgCl_4^{2-}$, the dichloride complex of $HgCl_2$, is the expected product with a large excess of Cl^-. Eventually the concentration of $HgCl_4^{2-}$ was found to decrease. At this time, the metallic Hg droplets lost their characteristic brightness and started to become white on the surface. Both the drop in $HgCl_4^{2-}$ and the white color were attributed to the formation of calomel on the surface of the Hg^0 droplets:

$$HgCl_4^{2-}(aq) + Hg^0(\ell) = Hg_2Cl_2(s) + 2\, Cl^-(aq)$$

The oxidation rate was found to increase approximately linearly with chloride concentration up to about 250 g/L Cl^-, at which point the rate decreased. At high enough Cl^- concentrations, the equilibrium concentration of oxygen decreases resulting in decreased reaction rate. The pH was found to have a significant effect on the oxidation rate, with significant rate increases at lower pH; the rate increase was more than expected just by the addition of more Cl^-. Yamamoto[41] found that addition of the chlorides KCl or $MgCl_2$ also increased the reaction rate.

Magalhães[40] proposed the following mechanism for the oxidation in aqueous solution:

$$Hg^0(\ell) = Hg^0(aq) \quad \text{(fast)} \quad (2.10)$$

$$Hg^0(aq) = Hg^{2+}(aq) + 2e^- \quad \text{(fast)} \quad (2.11)$$

$$Hg^{2+}(aq) + 2\ Cl^-(aq) = HgCl_2(aq) \quad \text{(slow)} \quad (2.12)$$

$$HgCl_2(aq) + 2\ Cl^-(aq) = HgCl_4^{2-}(aq) \quad \text{(fast)} \quad (2.13)$$

$$O_2(aq) + 2\ H^+ + 4\ e^- = 2\ OH^- \quad \text{(slow)} \quad (2.14)$$

The overall reaction can be written as:

$$2\ Hg^0(\ell) + O_2(aq) + 4\ H^+ + 4\ Cl^-(aq) = 2\ HgCl_2(aq) + 2\ H_2O \quad (2.15)$$

or in basic solution:

$$2\ Hg^0(\ell) + O_2(aq) + 2\ H_2O + 4\ Cl^-(aq) = 2\ HgCl_2(aq) + 4\ OH^- \quad (2.16)$$

This overall reaction shows that O_2 is the active oxidant. This mechanism is consistent with their observation that the pH increased during the course of the reaction (due to formation of OH^-). The positive effect of lower pH is also consistent – Eq. (2.14) will be faster with increased H^+ concentration. These authors also state that the oxidation reaction may actually occur at the surface of the Hg^0 droplet and that their experiments could not distinguish between these two possibilities. The rates of both reactions (2.12) & (2.13) should be increased by increases in Cl^- concentration as was found.

The oxidation of dissolved and liquid elemental mercury in oxygenated water with chloride present was studied by Amyot[42] The reactions were performed in the dark to eliminate photochemical reactions. The chloride present was added as KCl; no chlorine with oxidizing potential such as Cl_2 was added. Total Hg concentrations were in the range 20-100 nM (0.004-0.020 mg/L); Hg^0 solubility in oxygen-free water at 25 °C is about 284 nM (0.057 mg/L).[9] Chloride concentrations were varied from zero to 500 μM (17.7 mg/L). In this work, oxidized Hg was considered to be the sum of Hg(I) and Hg(II) concentrations. Oxygen concentrations were maintained by contacting the stirred test solutions with air.

In solutions containing dissolved Hg^0 only with no liquid elemental Hg^0 (droplets), the rate of Hg^0 oxidation by O_2 in the presence of chloride was essentially zero. However, rapid oxidation of Hg^0 occurred when Hg metal was present. The rate of oxidation

increased with increased concentration of chloride. The rate of oxidized mercury creation was also found to be a function of the mercury droplet surface area. The oxidation rate eventually decreased due to the accumulation of oxidation products on the Hg^0 metal surface. The absence of O_2 resulted in no oxidation as expected.

2.3.2 Oxidation in the Ontario Hydro Sampling Train

Laudal[15,36] and Linak[43] reported on tests of the Ontario Hydro sampling train,[39] which uses three impingers containing 10 wt% KCl solution to trap oxidized (Hg^{2+}) mercury. They found that the presence of Cl_2 resulted in statistically significant amounts of Hg^{2+} even though only Hg^0 was present in the test gas. They also found that the presence of SO_2 in the test gas decreased the amount oxidized. Cauch[44] specifically tested the Ontario Hydro method to quantify the effect of Cl_2 on the measured Hg^{2+}. Their results brought into question many of the results reported for homogeneous vapor phase oxidation of mercury because the Ontario Hydro sampling train or other sampling trains with potential biases had been used. The presence of SO_2 in the gas again eliminated the interference of Cl_2 on the Hg^{2+} measurement. Addition of sodium thiosulfate $Na_2S_2O_3$, which is a reducing agent, also eliminated the effect of Cl_2. Chlorine was postulated to be removed by these overall reactions:

$$SO_2 + Cl_2 + 2\,H_2O = H_2SO_4 + 2\,HCl \quad (2.17)$$

$$2\,Na_2S_2O_3 + Cl_2 = Na_2S_2O_6 + 2\,NaCl \quad (2.18)$$

Cauch[44] gives a mechanism for Cl_2 oxidation of Hg^0:

$$Cl_2(aq) + H_2O = HClO(aq) + H^+(aq) + Cl^-(aq) \quad (2.19)$$

$$HOCl(aq) = H^+(aq) + OCl^-(aq) \quad (2.20)$$

$$Hg^o(aq) + OCl^-(aq) = Hg^{2+}(aq) + Cl^-(aq) + 2\,OH\text{-}(aq) \quad (2.21)$$

They state that these reactions favor formation of hypochlorite, OCl^-, because the pH is greater than three and Cl^- concentration is low at 1000 ppm; therefore, OCl^- is the likely oxidizing species. However, the concentration of Cl^- in the Ontario Hydro sampling train is 1 N, or 35453 mg/L (ppm). Zhao[45] studied the absorption of element Hg^0 from the vapor into a solution of hypochlorite and found that the active oxidizing species was probably aqueous Cl_2:

$$Hg^o(aq) + Cl_2(aq) \rightarrow products \quad (2.22)$$

They did not explicitly name a product; $HgCl_2$ and Hg_2Cl_2 are the possible products. Aqueous Cl_2 is the likely oxidant because low pH (high H^+) and high Cl^- both increased the rate of absorption and oxidation of Hg^0. Both high Cl^- and high H^+ force reaction (2.19) towards Cl_2. Reaction (2.20) also favors HOCl over OCl^- at low pH, so OCl^- is not likely to be the active oxidant.

Zhao[46] studied elemental mercury vapor absorption in aqueous solutions containing Hg^{2+} added as $HgCl_2$. The products of the reaction of Hg^0 and Hg^{2+} were not stated, but some form of Hg^{1+} such as Hg_2Cl_2 must be the product. All chlorides, including NaCl, KCl, $FeCl_3$, were found to inhibit Hg^0 removal by Hg^{2+}. This result supports the basis for the KCl impingers to remove Hg^{2+} but not Hg^0 in the Ontario Hydro sampling system. Excess Cl^- reduces the amount of $Hg^{2+}(aq)$ in solution by forming the stable $HgCl_3^-$ and $HgCl_4^{2-}$ complexes of $HgCl_2$.

HCl at 0.9M was found to actually result in an increase in the Hg^0 content of the vapor indicating that Hg^{2+} was reduced. This result is interesting in that HCl is apparently acting as a reducing agent; if Hg^{2+} was reduced to Hg^0, then HCl must have been oxidized to Cl(+1). The following overall reaction forming the oxidized Cl(+1) species HOCl shows this reduction:

$$Hg^{2+}(aq) + HCl(aq) + H_2O = Hg^{o}(aq) + 2\ H^{+}(aq) + HOCl(aq) \qquad (2.23)$$

The inclusion of O_2 resulted in a slight removal of Hg^0 from the vapor indicating that the reduction of HCl did not occur in the presence of O_2. Rather, some Hg^0 was oxidized by the Hg^{2+} in solution. Other acids (HNO_3, H_2SO_4) were found to increase the rate of Hg^0 oxidation and removal.

2.3.3 Oxidation in Nitric Acid

Elemental mercury metal is readily oxidized by concentrated (~5M) nitric acid (HNO_3) to form Hg^{2+} ions while nitrate is reduced to NO_x gases and probably also nitrous acid HNO_2.

3.0 MODELING METHODS

The oxidation of elemental Hg^0 in the melter off-gas system could occur in the gas phase, the liquid phase, or both. The development of three models is anticipated:

1. Homogeneous gas-phase oxidation.
2. Liquid-phase oxidation.
3. Combined homogeneous gas-phase oxidation and liquid-phase oxidation.

In this preliminary work, an initial examination of the homogeneous gas phase oxidation has been performed to compare the proposed model chemistry to the ESCM melter data. The liquid phase oxidation has not been simulated except to demonstrate that the OLI software chemistry can generate all oxidation states of Hg seen experimentally. A preliminary combined model has also been generated to show that the gas phase reaction product composition, when combined with the approximate condensate composition, would result in the speciation of mercury reported in the literature.

3.1 BACKGROUND

Mercury would be fed to DWPF melter as an insoluble oxide (HgO in the Hg^{2+} oxidation state) under the proposed flowsheet modifications, and essentially 100% of the mercury fed would be volatilized as the elemental mercury vapor (zero oxidation state) during the calcination/fusion process. The mercury vapor is then presumed to undergo oxidation reactions (back to either +1 or +2 oxidation state) in the melter vapor space and downstream of the melter including the condensate tank. As summarized in Section 2.0, the literature on the oxidation kinetics of mercury is quite extensive in scope, ranging from the homogeneous gas-phase reactions to the heterogeneous liquid-phase reactions involving the solid-surface reactions.[18,42] However, most of the literature data are concerned with either the oxidation of mercury in the coal-fired power plant flue gases or various speciation reactions of mercury under diverse environmental conditions, including methylation of divalent mercury. The only literature data found to be related to the mercury emission from a glass melter were taken during the ESCM tests at PNL;[1] of particular relevance to DWPF are the mercury speciation data given in Table 2-5 for the condensate samples taken under different operating conditions.

3.2 HOMOGENEOUS OXIDATION IN THE GAS PHASE

The mercury oxidation model developed in this study was calibrated using these ESCM data. However, the model itself was developed based on the most recent intrinsic kinetic data available in the literature for the reactions between mercury and chloride species. Particularly, only those kinetic data taken under the post-flame conditions of coal-fired power plants were used in this study mainly due to the fact that the temperature range of these data is inclusive of those typically encountered in the melter vapor space and the off-gas header leading to the quencher. The following section describes the overall approach taken to model the complicated network of mercury speciation reactions that

are expected to occur in the melter and off-gas system along with several key assumptions made to develop a simple model that could serve as a useful scoping tool.

3.2.1 Modeling Approach

The schematic of the ESCM system is shown in Figure 3-1.[1] It has a 9-in by 9-in square cross-sectional area melter and its off-gas components are similar to those of the DWPF melter, consisting of a quencher, a condensate tank, a condenser and a HEPA filter. A key difference between the two off-gas systems is that the DWPF system has additional components like the Steam Atomized Scrubbers (SAS) and the HEME before and after the condenser, respectively, mainly to capture semi-volatile species such as CsCl. As far as the mercury speciation reactions are concerned, the ESCM or DWPF system can be divided into three distinct reaction zones. The first is the cold cap where the water portion of the slurry feed is converted into steam, and the remaining dry feed components are converted into glass and calcine gases. In this study, a high-temperature thermodynamic equilibrium software called FactSage v6.0 was used to calculate the composition of the volatile species from Zone 1.[47]

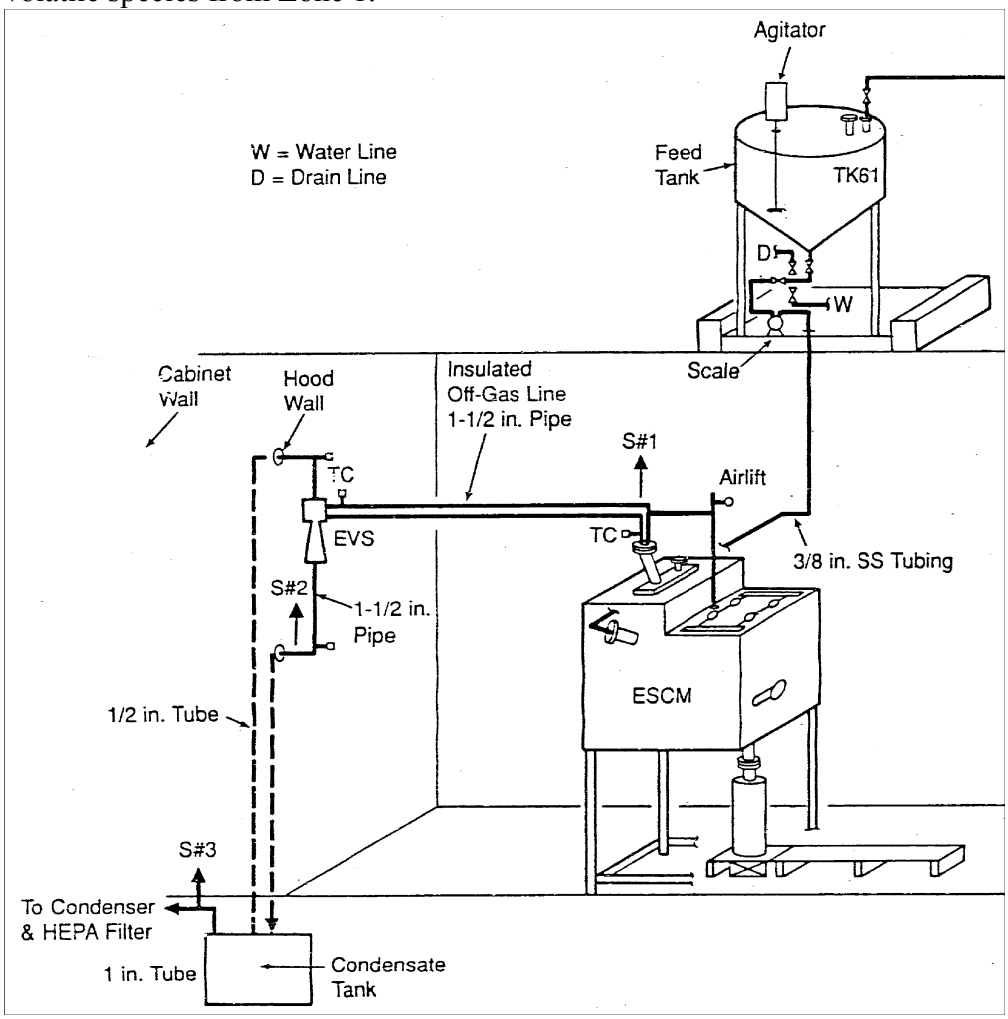

Figure 3-1. Schematic of ESCM and Off-Gas System

The calcine gases enter the second reaction zone along with the mercury vapor and volatile salts such as the chlorides and borates of alkali metals generated in Zone 1. The second reaction zone includes the vapor space of the melter and the off-gas header leading to the quencher, where those species volatilized from the melter mix with steam and air and further react. The third reaction zone resides inside the quencher and the condensate tank, where steam and volatile salts are condensed and may further react in the liquid phase. It would be necessary to model all three reaction zones in order to have a relatively complete description of how mercury would speciate throughout the ESCM or DWPF melter off-gas system. However, the scope of this task is limited to only the first two reaction zones; the liquid-phase reactions in Zone 3 were excluded because they were deemed less important than the gas-phase reactions in Zone 2 for the reasons given next.

3.2.2 Characteristics of Off-Gas Carryover

The carryover of materials into the off-gas can occur via two very different mechanisms; physical entrainment and vapor phase transport (or volatilization). Both feed and glassy materials can get airborne by physical entrainment aided in part by the pulling of the exhauster and remain as solids throughout the off-gas system. The entrained particulates, whose mean particle size is greater than 1 μm, account for much of the particle loading in the melter exhaust but over 90% of them are routinely scrubbed out in the quencher.[48]

On the other hand, alkali salts of chloride and borate and mercury are transported into the off-gas due to their volatility at the melt temperature but later condense as off-gas gets cooled and further quenched. Upon condensation, these semi-volatile salts would become primarily submicron-sized aerosols that are difficult to remove using an ejector venturi scrubber like the DWPF Quencher. As a result, the majority of the semi-volatile salts and mercury will remain in the gas stream downstream of the quencher, which means that the peak of the particle size distribution curve would shift from > 1 μm to < 1 μm after the quenching. The evidence for this shift was seen in the off-gas data taken at the inlet and outlet of the Quencher during the Large Slurry Fed Melter (LSFM) runs.[49]

Furthermore, the analysis of recent DWPF SAS deposit samples showed that ~8% of the mercury found in the deposit became water-soluble after ~3 days of intermittent shaking.[5] This result is in good agreement with the condensate sample data taken during the ESCM Tests 1 and 2, which showed that ~10% of the mercury present was soluble (Table 2-5). This agreement between two very different sample results regarding the partitioning of mercury between soluble and insoluble fractions suggests that much of the mercury chlorination may take place in the gas-phase upstream of the quencher and the resulting chlorinated mercury species become sub-micron sized aerosols upon condensation in the off-gas line or the quencher and pass right through the condensate tank vapor space. In DWPF, most of these semi-volatile aerosols are then removed in the SASes, the condenser and the HEME and eventually are returned to the condensate tank.

If this picture of the fate of mercury just described were correct, it would mean that the extent of further oxidation of mercury in the liquid phase of the condensate tank should be small compared to that of the gas-phase oxidation occurring in the melter vapor space. Based on this premise, the liquid-phase reactions of Zone 3 were ignored in this preliminary study except to perform two simplified simulations of contacting the off-gas from Zone 2 with a typical DWPF condensate (see Section 4.3).

3.2.3 Model Assumptions

The following simplifying assumptions were made to model the oxidation of mercury in the melter off-gas system:

1. The composition of calcine gases produced during the melting/fusion process is at equilibrium with those of the condensed phases at 1,150 °C (Zone 1).
2. Due to thermal radiation shine, the measured melter vapor space temperature is 100 °C higher than the actual gas temperature (Zone 2).
3. The chemical components of the melter exhaust are in equilibrium at the melter vapor space gas temperature except for those chloride-containing species that are not tied to the alkali metals (Zone 2).
4. Chloride atoms that are predicted to couple with alkali metals are not available for the chlorination of mercury (Zone 2).
5. The molar ratio of Cl_2 to Cl decreases linearly with increasing temperature between 550 and 750 °C (Zone 2).

3.2.4 Homogeneous Gas-Phase Oxidation Model

The elementary reactions shown in Reactions (3.1)-(3.4) were used to describe the gas-phase chlorination of mercury in Zone 2:

Table 3-1 Rate Constants of Zone 2 Oxidation Reactions of Mercury

Reaction No.	Zone 2 Reactions:	2^{nd} Order Rate Constants (cm^3 $molecules^{-1}$ sec^{-1})	Temperature (K)
(3.1)	$Hg^0 + Cl + M \rightarrow HgCl + M$	$k_1 = 6.0 \times 10^{-11}$	398-673
(3.2)	$HgCl + Cl + M \rightarrow HgCl_2 + M$	$k_4 = 4.0 \times 10^{-12}$	398-673
(3.3)	$HgCl + Cl_2 \rightarrow HgCl_2 + Cl$	$k_3 = 1.2 \times 10^{-11}$	423-673
(3.4)	$Cl + Cl + M \rightarrow Cl_2 + M$	$k_4 = 5.5 \times 10^{-33}$	423

The oxidation of mercury is initiated by the Cl atoms combining with the elemental mercury vapor via Reaction (3.1) to form mercurous chloride (+1 oxidation state). The Cl atoms further oxidize mercury from mercurous to mercuric chloride (+2 oxidation state) via Reaction (3.2). Reaction (3.3) was added to account for the effect of temperature on the speciation of chlorine; formation of Cl_2 is favored over Cl atoms at low temperatures, while formation of Cl atoms is favored over Cl_2 at high temperatures. The formation of Cl_2 by the recombination of Cl atoms via Reaction (3.4) would slow down Reactions

(3.1) and (3.2) and accelerate Reaction (3.3). However, Reaction (3.4) was excluded from the model, since its rate constant is many orders of magnitude smaller than the other reactions and the concentration of Cl atoms will be nowhere near high enough under normal circumstances to overcome such a large deficit in the rate constant.

The 2nd order rate constants used in the model were taken from a recent study using the laser photolysis/laser induced fluorescence (LP/LIF) technique.[18] It is noted that the upper temperature bounds for the rate constants of Reactions (3.1) to (3.3) are 50 and 100 °C lower than the estimated gas temperatures in the ESCM vapor space (Test 3) and the DWPF melter vapor space, respectively. As stated earlier, the temperature ranges are low since they were specifically derived under the post-flame conditions of coal-fired power plants. It is implicitly assumed here that these rate constants can be extrapolated to the temperature regions of interest to this study.

The concentrations of [Hg], [HgCl], [$HgCl_2$], [Cl] and [Cl_2] were found as a function of time by solving the following five rate equations simultaneously:

$$\frac{d[Hg]}{dt} = -k_1[Hg][Cl] \tag{3.5}$$

$$\frac{d[Cl]}{dt} = -k_1[Hg][Cl] - k_2[HgCl][Cl] + k_3[HgCl][Cl_2] \tag{3.6}$$

$$\frac{d[HgCl]}{dt} = k_1[Hg][Cl] - k_2[HgCl][Cl] - k_3[HgCl][Cl_2] \tag{3.7}$$

$$\frac{d[HgCl_2]}{dt} = k_2[HgCl][Cl] + k_3[HgCl][Cl_2] \tag{3.8}$$

$$\frac{d[Cl_2]}{dt} = -k_3[HgCl][Cl_2] \tag{3.9}$$

where the subscript *i* of each rate constant corresponds to Reactions (3.*i*) in Table 3-1.

Since practically all of the mercury fed would be volatilized, the initial concentration of mercury, $[Hg]_o$, for Zone 2 reactions is known, whereas both $[HgCl]_o$ and $[HgCl_2]_o$ are zero. Therefore, in order to solve Eqs. (3.5)-(3.9), the initial concentrations of [Cl] and [Cl_2] must be known, and the strategy used to find $[Cl]_o$ and $[Cl_2]_o$ is as follows:

1. Run FactSage model by using the sum of calcine gases, free H_2O of the feed, and air inleakage as the input to calculate the equilibrium melter exhaust composition at the measured melter vapor space temperature.
2. Calculate the total Cl atoms that are predicted not to couple with alkali metals, e.g., HCl, Cl, Cl_2, $HgCl_2$, etc.
3. Calculate the equilibrium Cl_2/Cl ratio as predicted by the FactSage model.

4. Assume a fraction of the total non-alkali-binding Cl atoms calculated in Step 2 that exist as either Cl or Cl_2.
5. Assume a percent approach to the equilibrium Cl_2/Cl ratio.
6. Solve for $[Cl]_o$ and $[Cl_2]_o$ based on the assumed settings of Steps 4 and 5.
7. Run Zone 2 oxidation model under ESCM Test 1 conditions at 750 ^oC.
8. Check if the calculated $HgCl/HgCl_2$ ratio matches the experimental data, i.e., ~9.
9. If so, move on to Step 10. If not, repeat Steps 4-8.
10. Repeat Steps 1-8 under ESCM Test 3 conditions at 550 ^oC and target $HgCl/HgCl_2$ ratio of ~1.
11. Repeat Steps 1-3 under DWPF SB5 conditions at 650 ^oC vapor space temperature.
12. Set the fraction of total Cl atoms that are not tied to alkali metals but exist as either Cl or Cl_2 at the average of those values found for ESCM Tests 1 and 3 in Step 4.
13. Set the percent approach to the equilibrium Cl_2/Cl ratio at the average of those values found for ESCM Tests 1 and 3 in Step 5.
14. Run Zone 2 oxidation model under DWPF SB5 conditions.

The reasoning behind taking a percent approach to the equilibrium Cl_2/Cl ratio in Step 5 is that the equilibrium-predicted Cl_2 concentration will be much higher than the actual value based in part on the kinetics of its formation, as evidenced by the negligibly small rate constant for Reaction (3.4). So, the initial Cl_2/Cl ratio was reduced to a certain percentage of what is predicted by the equilibrium model. The basis for taking the average ESCM values in Steps 12 and 13 is the fact that the nominal indicated DWPF melter vapor space temperature (TI4085D) of 650 °C falls right in the middle of the two corresponding ESCM temperatures. If the ESCM temperature range were greater than 200 °C or the DWPF temperature fell outside the ESCM range, a linear interpolation or extrapolation might not be a good approximation.

3.3 AQUEOUS PHASE OXIDATION – OLI SOFTWARE

3.3.1 Mercury Compound Equilibria

3.3.1.1 Solution Equilibria

The aqueous equilibria of Hg^0, Hg^{2+}, and Hg_2^{2+} compounds at 25 °C are summarized in Table 3-2.[8-11,50-52] Note that the disproportionation reactions of Hg^{1+} are actually reduction-oxidation (redox) reactions. These literature values are those determined to be the "best available" by the reference authors. Both literature values and values calculated for the test cases using the OLI StreamAnalyzer software are given. There is very little literature data available at temperatures other than 25 °C, but these properties can be estimated in OLI. There is generally reasonable agreement between the literature values and those calculated using the StreamAnalyzer; the typical difference between the two are about a factor of two, which is actually quite good given the range of literature data.

The solubility product K_{sp} for $Hg_2Cl_2(s)$ in the OLI Public database was found to predict ~127 times greater solubility than the literature data. In order to correct this error, a private database called CALOMEL was created using Equation 22 from Marcus.[51]

Table 3-2 Mercury Species Equilibria

Not all equilibria are independent. Ionic species are all aqueous (aq).
Equilibrium constants K are based on species activities and are for 25 °C.

Liquid or Solid / Aqueous:	K (Literature)	K (OLI)
$Hg^{o}(\ell) = Hg^{o}(aq)$	3.0 x 10^{-7} m	1.30 x 10^{-7} m
$HgCl_2(s) = HgCl_2(aq)$	0.270 m	0.263 m
Disproportionation of Hg(I):	**K (Literature)**	**K (OLI)**
$Hg_2^{2+} = Hg^{2+} + Hg^{o}(\ell)$	1.15 x 10^{-2}	1.15 x 10^{-2}
$Hg_2^{2+} = Hg^{2+} + Hg^{o}(aq)$	3.44 x 10^{-9} m	1.49 x 10^{-9} m
$Hg_2Cl_2(s) = HgCl_2(aq) + Hg^{\circ}(\ell)$	2.35 x 10^{-7} m	12.9 x 10^{-7} m
$Hg_2Cl_2(s) = HgCl_2(aq) + Hg^{\circ}(aq)$	7.10 x 10^{-14} m^2	16.8 x 10^{-14} m^2
$Hg_2Cl_2(s) + 2Cl^{-} = HgCl_4^{2-} + Hg^{\circ}(\ell)$	2.05 x 10^{-5} m^{-1}	5.19 x 10^{-5} m^{-1}
Solubility product (K_{sp}) of calomel:	**K (Literature)**	**K (OLI)**
$Hg_2Cl_2(s) = Hg_2^{2+} + 2Cl^{-}$	1.43 x 10^{-18} m^3	1.53 x 10^{-18} m^3
Solubility of calomel as undissociated molecule:	**K (Literature)**	**K (OLI)**
$Hg_2Cl_2(s) = Hg_2Cl_2(aq)$	3.34 x 10^{-6} m	Hg_2Cl_2(aq) species not in OLI
Hg(I) hydroxides:	**K (Literature)**	**K (OLI)**
$Hg_2^{2+} + H_2O = Hg_2OH^{+} + H^{+}$	3.98 x 10^{-5} m	2.07 x 10^{-5} m
$Hg_2OH^{+} + H_2O = Hg_2(OH)_2 + H^{+}$	not found	no K-value in OLI

Hg(II) with chlorides:	K (Literature)	K (OLI)
$Hg^{2+} + Cl^{-} = HgCl^{+}$	5.75 x 10^{+6} m^{-1} to 22.0 x 10^{+6} m^{-1}	15.8 x 10^{+6} m^{-1}
$HgCl^{+} + Cl^{-} = HgCl_2(aq)$	2.51 x 10^{+6} m^{-1}	4.67 x 10^{+6} m^{-1}
$HgCl_2(aq) + Cl^{-} = HgCl_3^{-}$	6.70 m^{-1}	10.2 m^{-1}
$HgCl_3^{-} + Cl^{-} = HgCl_4^{2-}$	13.0 m^{-1}	3.95 m^{-1}
$Hg^{2+} + 2Cl^{-} = HgCl_2(aq)$	1.45 x 10^{+13} m^{-1} to 18.2 x 10^{+13} m^{-1}	7.36 x 10^{+13}
$Hg^{2+} + 4Cl^{-} = HgCl_4^{2-}$	1.30 x 10^{+15} m^{-4} to 16.3 x 10^{+15} m^{-4}	2.96 x 10^{+15} m^{-4}

All of these Hg^{+2} species are described in the literature as chloride complexes of Hg^{+2}:

Hg(II) hydroxides:	K (Literature)	K (OLI)
$Hg^{2+} + 2H_2O = Hg(OH)_2(aq) + 2H^{+}$	2.24 x 10^{-6} m^2	0.654 x 10^{-7} m^2
$Hg^{2+} + H_2O = HgOH^{+} + H^{+}$	8.13 x 10^{-4} m	3.91 x 10^{-4} m
$Hg(OH)_2(aq) + H_2O = Hg(OH)_3^{-} + H^{+}$	1.66 x 10^{-15} m	0.872 x 10^{-15} m
$HgO(s) + H_2O = Hg(OH)_2(aq)$	5.80 x 10^{-4} m	1.82 x 10^{-4} m

Hg(II) nitrate and sulfate are totally dissociated except at saturation and high ionic strength.

It should also be noted that the species activities, calculated from the concentrations and the activity coefficients from OLI, must be used and not just the species concentrations. The species concentrations are adequate only when approaching infinite dilution.

Some general notes about mercury species equilibria are:

- Elemental Hg^0 is only slightly soluble in oxygen-free water, although much more soluble than most metals.
- The solubility of Hg^0 in oxygenated water approximately equals that of HgO.
- $HgCl_2$ is very soluble in water and does not dissociate appreciably.
- $HgCl_2$ with excess Cl^- forms the very stable complexes $HgCl_3^-$ and $HgCl_4^{2-}$.
- Calomel Hg_2Cl_2 is extremely insoluble in water.
- Hg_2Cl_2 disproportionates into $Hg^0(s)$ and $HgCl_2(aq)$.

3.3.2 Liquid-Vapor Equilibria

The solubility and Henry's law constants as functions of temperature for Hg^0 and $HgCl_2$ are shown in Figure 3-2-Figure 3-3.[9,53] Both literature data and model predictions are shown. At below 80 °C, the predicted solubility of Hg^0 is significantly low, while the predicted vapor pressure is high. As a result, the predicted Henry's law constant is significantly high at below 80 °C.

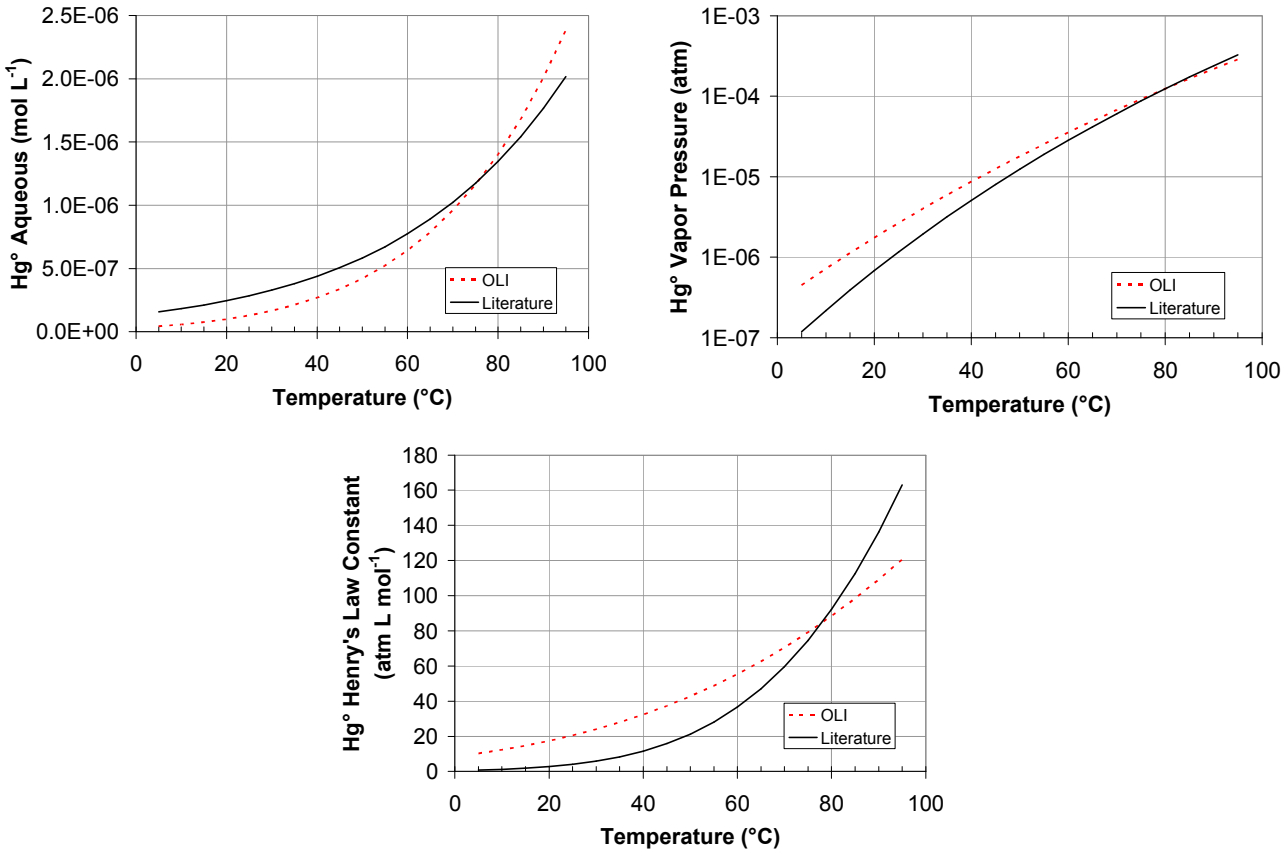

Figure 3-2 Solubility, Vapor Pressure and Henry's Law Constant for Hg^0 in Water

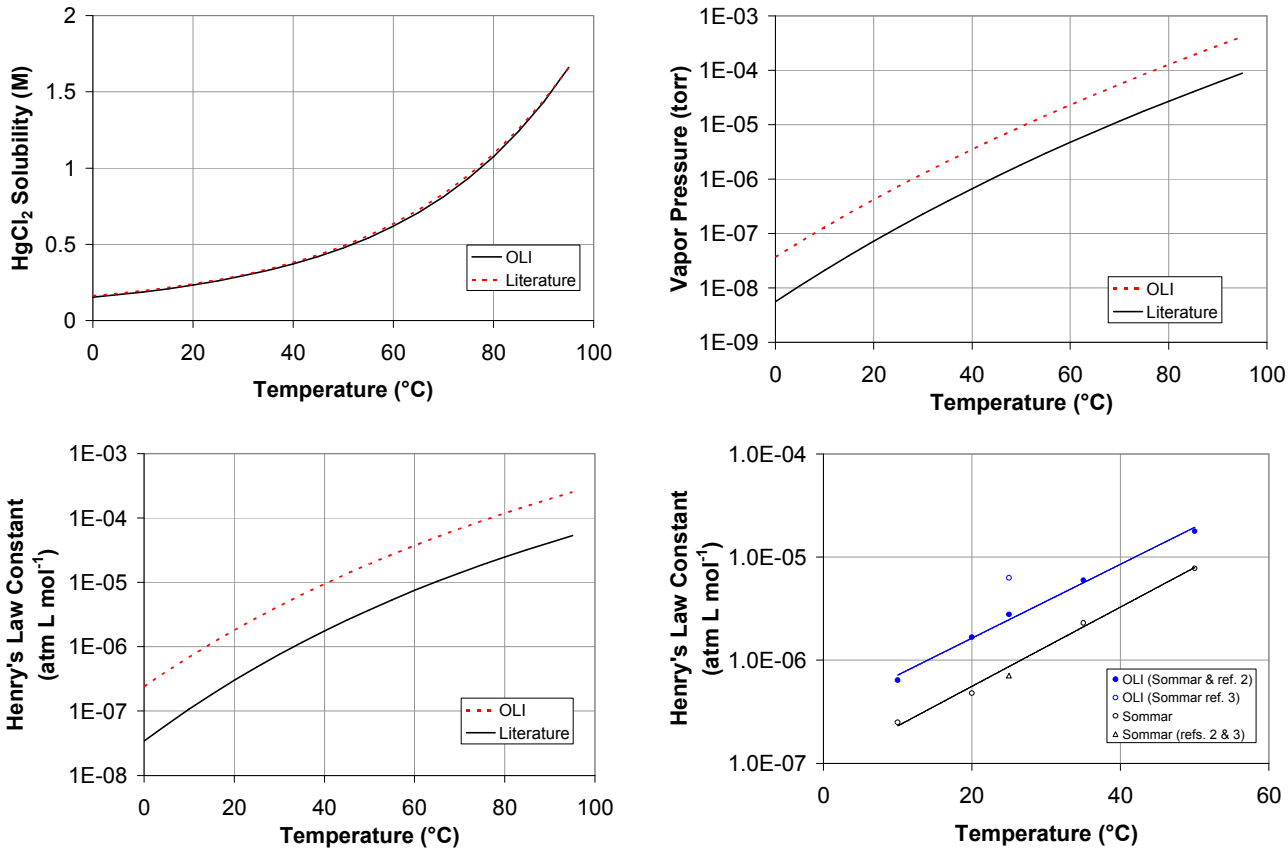

Figure 3-3 Solubility and Henry's Law Constant for $HgCl_2$ in Water

At 25 °C, the predicted solubility is about 45% of the literature value, while the vapor pressure is about 2.2 times that in the literature. As with the equilibrium constants, the literature values and OLI predictions are also within about a factor of two.

The solubility of $HgCl_2$ is predicted accurately by OLI, but the vapor pressure is 4.7-6.6 times higher than given in the literature. The literature value for the Henry's law constant for $HgCl_2$ in Figure 3-3 was calculated from solubility and vapor pressure data from two sources. The predicted constants from OLI are 4.7-7 times higher. OLI predictions were also generated for data tabulated by Sommar[54] for pH 0.3-1.5 and pCl (-log[Cl^-]) of 2.7-3.7. The predictions were 2.2-3.9 times larger.

3.3.3 Aqueous Redox Reactions

The OLI software has the capability of handling some reduction-oxidation (redox) reactions in the aqueous phase. This redox capability is equilibrium based, so there is no consideration for reaction kinetics. In OLI, redox reactions can be turned on or off for individual elements. In StreamAnalyzer, individual redox reactions cannot be easily turned on or off; in the OLI ESP flowsheet modeling software, model files can be created with specific reactions "turned off".

Oxidizers present in the melter off-gas are Cl_2, O_2, NO, and NO_2. The roles of NO and NO_2 in Hg chemistry are not clear. Sulfur dioxide SO_2 can oxidize Hg, but with Cl_2 it has been shown to the suppress oxidation of Hg^0 by Cl_2 by reducing Cl_2 to Cl^-. Hydrochloric acid HCl is not an oxidizer, but provides chloride to the equilibria with oxidized Hg (as does NaCl and other chlorides). In the reactions below, the oxidation states of the elements are shown above the reactions.

Elemental Hg Oxidation by Oxygen

$$\overset{0}{2\,Hg}(\ell) + \overset{0}{O_2}(aq) = \overset{+2\ -2}{2\,HgO}(s) \qquad (3.10)$$

This reaction takes place in solution between Hg^0 liquid metal and dissolved oxygen. In the OLI software with Hg redox turned on, oxygen always oxidizes Hg. In the presence of less than stoichiometric O_2 and with Cl^- present, Hg^0 can be partially oxidized to the +1 oxidation state (Hg_2^{2+}).

A shortcoming of the OLI software is that it applies equilibrium between all phases, so the large excess of O_2 in the off-gas stream effectively oxidizes all oxidizable species in solution even if there are actually reaction kinetics or mass transfer limitations. Therefore, to handle the actually limited oxidizing power of O_2 in this situation, the amount of O_2 must be limited. At any time, the amount of O_2 in solution cannot exceed its solubility, so that limiting the transfer of O_2 from the gas to the aqueous phase should be a method for limiting oxidation by O_2.

Mercuric oxide solid can react with chloride ions to give mercuric chloride:

$$HgO(s) + 2\,Cl^- + H_2O = HgCl_2(aq) + 2\,OH^- \qquad (3.11)$$

This is not a redox reaction. The oxidation of $Hg^0(\ell)$ in solution is significantly accelerated by the presence of Cl^- that produces $HgCl_2$ from HgO. $HgCl_2$ and its Cl^- complexes are extremely stable in solution.

Elemental Hg Oxidation by Chlorine

$$\overset{0}{Hg^\circ}(\ell) + \overset{0}{Cl_2}(aq) = \overset{+2\ \ 2(-1)}{HgCl_2}(aq) \qquad (3.12)$$

This reaction probably does not occur as written by this stoichiometry, but by a more complex series of reactions. Less than stoichiometric amounts of Cl_2, like O_2, result in partial oxidation of Hg^0 to the +1 oxidation state. The dissolution of Cl_2 in water is a disproportionation that forms hypochlorous acid (HOCl) and HCl, which are in the +1 and -1 oxidations states, respectively:

$$\overset{0}{Cl_2}(aq) + \overset{2(+1)\,-2}{H_2O} = \overset{+1\ -2\ +1}{HOCl}(aq) + \overset{+1}{H^+} + \overset{-1}{Cl^-} \quad (3.13)$$

Chlorine can also oxidize water to form O_2, as shown by this overall reaction:

$$2\,\overset{0}{Cl_2}(aq) + 2\,H_2O = 4\,\overset{4(-1)}{H^+} + 4\,\overset{0}{Cl^-} + O_2 \quad (3.14)$$

With Cl redox turned on, OLI's equilibrium calculations always result in all excess Cl_2 reacting with water to form O_2, which may be thermodynamically favorable, but not kinetically significant. In OLI, oxidation of Hg^0 by Cl_2 is exactly equivalent to oxidation by Cl_2 of H_2O to make O_2, followed by oxidation of Hg^0 by the O_2.

Reactions with SO_2

Generally, SO_2 acts a reductant for most species of interest, but in some cases appears to increase the amount of Hg^0 oxidized. Hutson[55] has shown that in scrubbing of Hg^0 using $NaClO_2$ as an oxidant, the addition of some SO_2 to the vapor enhances scrubbing and oxidation of Hg^0, but that higher concentrations of SO_2 then result in less scrubbing and oxidation. Scott[38] has shown that SO_2, or S(IV), can reduce Hg^{2+} to Hg^0 in both the gas and liquid phases. The proposed reactions in solution producing Hg^0 are:

$$SO_2 + H_2O = 2\,H^+ + SO_3^{2-} \quad (3.15)$$

$$Hg^{2+} + SO_3^{2-} = HgSO_3(aq) \quad (3.16)$$

$$HgSO_3(aq) + SO_3^{2-} = Hg(SO_3)_2^{2-}(aq) \quad (3.17)$$

$$HgSO_3 + H_2O = Hg^0 + H_2SO_4 \quad (3.18)$$

Mercuric sulfite [S(IV)] and possibly a disulfite complex are proposed as intermediates. In aqueous solutions, the formation of an Hg•S(IV) intermediate complex followed by decomposition to form Hg^0 has been proposed to explain the reemission of Hg as Hg^0 from scrubbers that remove Hg^{2+}.[56,57] Zhao[58] has shown that SO_2 inhibits the oxidation of Hg^0 by Cl species in the gas phase when water is present, but that no inhibition occurs when water is absent.

Sulfur dioxide will act as a reductant for oxidized mercury or chlorine. In OLI, Cl_2 and SO_2 preferentially and thus Cl_2 does not oxidize Hg^0. This redox chemistry reflects the actual experimentally determined chemistry. Cauch[44] showed that SO_2 reduces Cl_2 to chloride in solution, while sulfur is apparently oxidized to sulfuric acid:

$$\overset{0}{Cl_2} + \overset{+4}{SO_2} + 2\,H_2O = 2\,\overset{2(-1)}{HCl} + \overset{+6}{H_2SO_4} \quad (3.19)$$

However, excess SO_2 in OLI can oxidize Hg^0 to HgS, while sulfur itself disproportionates to S(-2) and S(+6):

$$\overset{0}{Hg^{o}} + 3\,\overset{3(+4)}{SO_2} + 2\,H_2O = \overset{+2\ -2}{HgS} + 2\,\overset{2(+6)}{H_2SO_4} \qquad (3.20)$$

This overall reaction is similar to that proposed by Scott[38] for a gas-solid surface catalyzed reaction of Hg^0 and SO_2. Therefore, like O_2, the effect of sulfur redox in OLI must be carefully checked.

4.0 RESULTS AND DISCUSSION

4.1 HOMOGENEOUS OXIDATION MODELING OF ESCM TESTS

The results of Zone 1 and 2 model runs are presented in this section along with their implications on the DWPF melter off-gas system operation. It should be noted that these results and discussions are only preliminary and scoping in nature. Further substantiation of these results would require a more in-depth modeling study accompanied by the proof-of-the-principle experimental tests.

The Zone 1 and 2 models of the ESCM Tests 1 and 3 are presented. As described earlier, the Zone 2 model contains two critical parameters pertaining to the partitioning of Cl/Cl_2 among non alkali-metal binding chloride atoms (Steps 4 and 5 in Section 1). The values of these parameters were determined by matching the calculated insoluble-to-soluble mercury ratios ($HgCl/HgCl_2$) with the measured data shown next:

	Test 1	Test 3
Target $HgCl/HgCl_2$ (mole/mole)	9	1

4.1.1 ESCM Zone 1 Model

The input compositions for the FactSage equilibrium model are given in Table 4-1. The amount of free H_2O in each feed was estimated by matching the calculated slurry feed density using the following correlation with the measured value of 1.363:

$$\rho\,(g/ml) \;=\; 0.001024TS^2 - 0.08655TS + 3.1891 \qquad (4.1)$$

where TS is the wt% total solids between 40 and 50 wt%. The total solids content of the ESCM feeds thus estimated was 44 wt%. The two main differences between Tests 1 and 3 were that; (1) the melter was fed 2.8 times faster during Test 1 than Test 3 and (2) the melter vapor space was kept 200 ^{o}C cooler during Test 3 by turning off the lid heaters, i.e., 550 ^{o}C (Test 3) vs. 750 ^{o}C (Test 1). The rate of melter air inleakage was the same at 25 kg/hr in both tests. The molar ratio of Cl/Hg was 12, which means that regarding the chlorination of mercury, chloride was present in excess.

The results of the FactSage model runs at 1,150 °C are shown in Table 4-2. As expected, 100% of the mercury fed was predicted to volatilize as elemental mercury vapor. At 1,150 °C under equilibrium conditions, 100% of the chloride fed was also predicted to volatilize as either HCl or alkali chlorides at a ratio of 40:60, respectively. A negligible quantity of Cl atoms was also predicted to form but not Cl_2. It should be noted that the mercury and alkali chlorides became part of the off-gas carryovers due to their low vapor pressures at the melt temperature, and the model predictions do not include any solids that are physically entrained because such a prediction is beyond the scope of an equilibrium model.

Table 4-1 Input Compositions of ESCM Tests 1 and 3 Feeds for FactSage Model

insoluble solids	Test 1 mole/hr	Test 3 mole/hr	soluble solids	Test 1 mole/hr	Test 3 mole/hr
Fe(OH)3	2.452352	0.87584	Ca(COOH)2	0.209199	0.074714
Al(OH)3	1.58134	0.564764	Ca(NO3)2	0	0
MnO2	0.187459	0.06695	Co(COOH)2	0	0
CaF2	0.01532	0.005471	Co(NO3)2	0	0
Zeolite	0.183831	0.065654	CsCOOH	0	0
MgO	0.329237	0.117585	CsNO3	0.01074	0.003836
Hg	0.015466	0.005524	Cu(COOH)2	0	0
Ca3(PO4)2	0.003133	0.001119	Cu(NO3)2	0	0
Ni(OH)2	0.173392	0.061926	KCOOH	0.040002	0.014287
Cr(OH)3	0.02431	0.008682	KNO3	0	0
Cu2O	0.014106	0.005038	Mg(COOH)2	0	0
TiO2	0	0	Mg(NO3)2	0	0
SiO2	15.97875	5.706698	Mn(COOH)2	0.438436	0.156584
Na2O	2.813338	1.004763	Mn(NO3)2	0	0
ThO2	0	0	NaCl	0.185452	0.066233
Zn(OH)2	0	0	NaF	0.01513	0.005404
PuO2	0	0	NaCOOH	0.901518	0.321971
K2O	0	0	NaNO3	0.313552	0.111983
RuO2	0.019944	0.007123	NaNO2	0	0
RhO2	0	0	Ni(COOH)2	0	0
PdO	0	0	Ni(NO3)2	0	0
Ag2O	0	0	Pb(NO3)2	0	0
SrCO3	0	0	Pd(NO3)2	0	0
Cs2O	0	0	Sr(COOH)2	0.004293	0.001533
B2O3	1.906047	0.680731	Sr(NO3)2	0	0
Gd(OH)3	0	0	UO2(COOH)2	0	0
PbSO4	0	0	UO2(NO3)2	0	0
Li2O	3.102282	1.107958	Y(COOH)3	0	0
Y2(CO3)3	0	0	Y(NO3)3	0	0
ZrO2	0.107693	0.038462	Zn(COOH)2	0	0
CaCO3	0.05229	0.018675	Zn(NO3)2	0	0
CaSO4	0.024711	0.008825	Na2CO3	0	0
CaC2O4	0	0	Na2C2O4	0	0
Al2O3	0.183831	0.065654	Na2SO4	0.011842	0.004229
total insoluble (kg/hr)	1.850646	0.660945	total soluble (kg/hr)	0.198092	0.070747
			total dried feed (kg/hr)	2.048738	0.731692
			free H2O	145.1073	51.82404
			density (g/ml) =	1.363	1.363
			feed rate (L/hr) =	3.738	1.335
			air inleakage (kg/hr) =	25.17	25.17

Table 4-2 FactSage Equilibrium Model Results at 1,150 °C for ESCM Tests.

	Test1	Test 3		Test1	Test 3
PHASE: gas_ideal	mole/hr	mole/hr	PHASE: BSlag-liq#1	mole/hr	mole/hr
H2O	7.0504E+00	2.5331E+00	MgO	3.2920E-01	1.1758E-01
CO2	2.0746E+00	7.7209E-01	MnO	6.2588E-01	2.2353E-01
H2	1.8582E-01	6.6762E-02	Na2O	3.0331E+00	1.0866E+00
N2	1.6215E-01	5.7909E-02	SiO2	1.0409E+01	3.7340E+00
CO	1.2207E-01	4.5429E-02	CaO	2.4920E-01	1.0221E-01
HCl	7.3597E-02	2.5845E-02	Al2O3	9.7445E-01	3.4804E-01
NaCl	6.6210E-02	2.3868E-02	K2O	0.0000E+00	7.0874E-03
HF	4.4671E-02	0.0000E+00	NiO	8.1145E-02	2.6003E-02
LiCl	3.0862E-02	1.1125E-02	Fe2O3	4.1195E-02	1.2380E-02
SO2	2.1736E-02	7.8333E-03	B2O3	1.1249E+00	3.9981E-01
HBO2	1.6887E-02	5.9284E-03	MnSO4	1.1384E-07	4.4553E-08
Hg	1.5500E-02	5.5239E-03	NiSO4	1.4759E-08	5.1830E-09
H3BO3	1.0999E-02	3.8497E-03	Fe2(SO4)3	7.4929E-09	2.4676E-09
LiBO2	9.9590E-03	3.5891E-03	Na2SO4	5.5168E-07	2.1659E-07
CsCl	7.5577E-03	2.7149E-03	CaSO4	4.5326E-08	2.0373E-08
NaBO2	7.0700E-03	2.5479E-03	MgSO4	5.9877E-08	2.3437E-08
CsBO2	3.0862E-03	1.1083E-03	TOTAL:	1.6868E+01	6.0572E+00
(NaCl)2	2.4901E-03	8.9791E-04			
H2S	1.3239E-03	4.7567E-04	PHASE: pure liquids	mole/hr	mole/hr
FeCl2	5.3329E-04	1.8305E-04	Li2Si2O5_liquid	2.7849E+00	9.8637E-01
(LiCl)2	5.1449E-04	1.8552E-04	FeO_liquid	1.0075E+00	3.8516E-01
LiF	4.6795E-04	0.0000E+00	NaBO2_liquid	9.2125E-01	3.1665E-01
OBF	3.3912E-04	0.0000E+00	LiBO2_liquid	5.9209E-01	2.2797E-01
LiOH	3.3289E-04	1.2278E-04	Fe3O4_liquid	4.5394E-01	1.5523E-01
(HBO2)3	1.7524E-04	5.8382E-05	Ni_liquid	7.2281E-02	2.8874E-02
Fe(OH)2	1.3995E-04	5.0281E-05	Ni3S2_liquid	6.6343E-03	2.3414E-03
NaF	1.3432E-04	0.0000E+00	TOTAL:	5.8386E+00	2.1026E+00
NaOH	1.1969E-04	4.4143E-05			
SO	8.5064E-05	3.0656E-05			
KCl	0.0000E+00	8.0091E-05			
NiCl2	5.0994E-05	1.7503E-05			
KBO2	0.0000E+00	3.1902E-05			
COS	2.8576E-05	1.0635E-05			
HS	2.0934E-05	7.5328E-06			
CsOH	1.7840E-05	6.5567E-06			
S2	1.6668E-05	6.0070E-06			
MnCl2	1.6556E-05	6.1720E-06			
Na	1.5845E-05	5.8529E-06			
Ni(OH)2	1.1134E-05	4.0004E-06			
(CsCl)2	8.5726E-06	3.0696E-06			
Cl	2.9037E-06	1.0213E-06			
B2O3	1.2988E-06	4.4553E-07			
TOTAL:	9.9101E+00	3.5715E+00			

It is also noted that the predicted melt composition appears to be very reducing, as evidenced by the formation of FeO and sulfides such as Ni_3S_2. Since the actual feed was not that reducing, this is more likely the result of the single-stage cold cap modeling; all reducing agents were assumed to react with the rest of the feed at the same time at the melt temperature, whereas in reality the formate decomposes early on in the cold cap and therefore exerts much less reducing power in the later redox reactions. This difficulty has been overcome by taking a multistage modeling approach in describing the DWPF cold cap chemistry.[59] However, the reducing nature of the ESCM glasses does not impact the volatilization of mercury and chloride, which are the essential input components of the Zone 2 model.

4.1.2 ESCM Zone 2 Model

The Zone 2 model consisted of two parts. The first was the FactSage model to calculate the equilibrium compositions of the melter exhausts at the measured melter vapor space temperatures of 750 and 550 ^oC for Tests 1 and 3, respectively. The second part was the gas-phase kinetics model of mercury chlorination which further adjusted the equilibrium speciation of mercury. The input for the Zone 2 FactSage model included; (1) the ideal-gas output shown in Table 4-2, (2) free H_2O that volatilizes from the cold cap, and (3) the air inleakage to the melter. The flow rates of the latter two streams are given in Table 4-1.

The results of the FactSage model runs are shown in Table 4-3 under the heading EQUIL. As in the Zone 1 run at 1,150 °C, the 60:40 split of total chloride atoms between HCl and alkali metals, respectively, was generally maintained in Test 1, while at 200 °C lower in Test 3 equilibrium favors ~10% more chloride atoms to couple with alkali metals. The summary of gas-phase results given in Table 4-3 also show that equilibrium favors; (1) all of the chloride atoms that do not couple with alkali metals to be in the form of HCl with little or no Cl/Cl_2, and (2) the formation of Cl_2 over Cl even at 750 °C. This is why Steps 4 and 5 in Section 1 were necessary to force some of the equilibrium-predicted HCl into Cl and Cl_2 for the mercury chlorination reactions to proceed.

After a few trial-and-error runs, it was found that when the percent total chloride atoms not tied to the alkali metals that exist as either Cl atom or Cl_2 was set at 13.5%, and the percent approach to the equilibrium Cl_2/Cl ratio set at 1%, the initial concentrations of Cl and Cl_2 would be $1.0458x10^{-9}$ and $1.9455x10^{-11}$ mole/cm^3, respectively, for Test 1. Figure 4-1 shows that the calculated $HgCl/HgCl_2$ ratio would match the experimental value of 9 at these initial concentrations. It is noted that the kinetics of mercury chlorination is so fast that the reactions are essentially complete in 0.5 msec. Therefore, considering the fact that the estimated gas residence time in the ESCM vapor space was on the order of 5 seconds for Test 1, it may be concluded that the chlorination of mercury will be complete at the instant Cl and Cl_2 are formed. However, this study does not address the question of how atomic Cl and Cl_2 are formed in the first place. The five ordinary differential equations of the Zone 2 kinetic model (Eqs. 3.1-3.5) were solved simultaneously using the RK4 v3.0.[60]

Table 4-3 Results of Zone 2 FactSage and Kinetic Model Runs for ESCM Tests.

ESCM Run	Test 1	Test 1	Test 3	Test 3
Calculation Mode	EQUIL	EQUIL+KINETIC	EQUIL	EQUIL+KINETIC
Measured Melter VS T (°C)	750	750	550	550
Melter VS Gas T (°C)	650	650	450	450
PHASE: gas_ideal	mole/hr	mole/hr	mole/hr	mole/hr
H2O	1.5230E+02	1.5230E+02	5.4408E+01	5.4408E+01
N2	2.0048E+01	2.0048E+01	1.9944E+01	1.9944E+01
O2	5.1176E+00	5.1176E+00	5.2225E+00	5.2225E+00
CO2	2.1967E+00	2.1967E+00	8.1752E-01	8.1752E-01
HCl	1.0615E-01	9.4686E-02	2.4156E-02	2.8174E-02
HF	4.4662E-02	4.4662E-02	0.0000E+00	0.0000E+00
H3BO3	3.8110E-02	3.8110E-02	1.6995E-02	1.6995E-02
Hg	1.3582E-02	1.8272E-03	6.7329E-06	8.0808E-04
CsCl	7.8152E-03	7.8152E-03	1.1792E-05	1.1792E-05
HgCl	0.0000E+00	1.2031E-02	0.0000E+00	2.3873E-03
HgCl2	1.6472E-03	1.3712E-03	5.5167E-03	2.3281E-03
(CsCl)2	1.4134E-03	1.4134E-03	4.0371E-06	4.0371E-06
NaCl	1.2280E-03	1.2280E-03	1.9465E-07	1.9465E-07
LiCl	8.9557E-04	8.9557E-04	2.4872E-07	2.4872E-07
(NaCl)2	3.9462E-04	3.9462E-04	2.9414E-08	2.9414E-08
NO	3.5404E-04	3.5404E-04	1.3714E-05	1.3714E-05
HgO	2.7039E-04	2.7039E-04	4.1781E-07	4.1781E-07
(LiCl)2	2.3795E-04	2.3795E-04	6.2811E-08	6.2811E-08
NO2	1.2396E-05	1.2396E-05	5.9788E-06	5.9788E-06
(HBO2)3	1.3161E-05	1.3161E-05	9.5524E-06	9.5524E-06
Cl2	7.6885E-06	5.7647E-07	1.3981E-05	3.2323E-11
OH	7.4610E-06	7.4610E-06	1.0727E-08	1.0727E-08
Cl	4.1328E-06	3.1141E-06	4.3231E-08	3.1490E-11
TOTAL:	1.7988E+02	1.7987E+02	8.0439E+01	8.0443E+01
PHASE: condensed	mole/hr	mole/hr	mole/hr	mole/hr
NaCl (s)	5.9705E-02	5.9705E-02	2.6678E-02	2.6678E-02
LiNa(SO4) (s)	1.6537E-02	1.6537E-02	1.5339E-03	1.5339E-03
LiBO2 (s)	9.8507E-03	9.8507E-03	0.0000E+00	0.0000E+00
Li2SO4 (s)	6.5225E-03	6.5225E-03	6.7754E-03	6.7754E-03
CsCl (s)	0.0000E+00	0.0000E+00	3.8033E-03	3.8033E-03
TOTAL:	9.2615E-02	9.2615E-02	3.8791E-02	3.8791E-02
Summary of Gas-Phase Results				
% Cl tied to alkali metals	40	40	46	46
% Cl not tied to alkali metals	60	60	54	54
% Cl as Cl-Cl2 in non-alkali Cl	0.02	13.50	0.08	20.00
% approach to equilibrium	-	1.00	-	0.22
ratio Cl as Cl2/Cl atom	3.721	0.037	646.804	1.423
initial conc [Cl]o (mole/cm3)	3.0335E-13	1.0458E-09	9.0589E-15	6.0915E-10
initial conc [Cl2]o (mole/cm3)	5.6434E-13	1.9455E-11	2.9297E-12	4.3340E-10
calculated HgCl/HgCl2	0.0	8.8	0.0	1.0
Target HgCl/HgCl2	-	9	-	1
Hg oxidation (% total Hg)	12	86	100	85

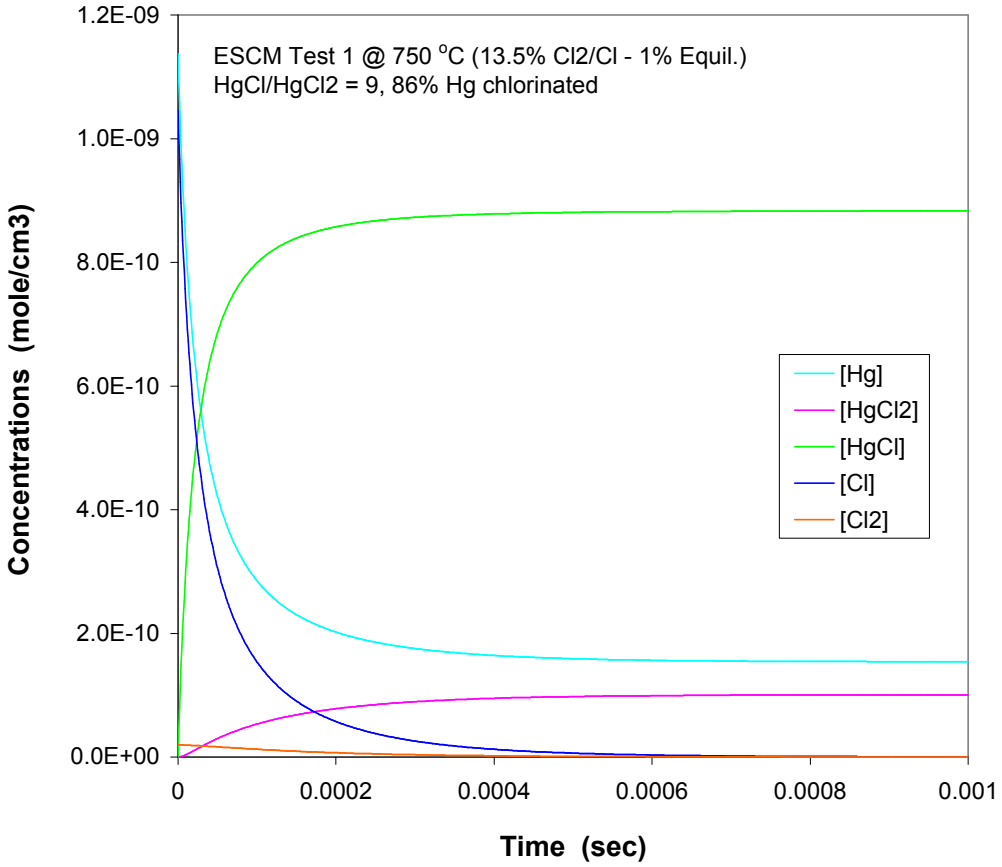

Figure 4-1 Concentration Profiles of Mercury Chlorination Reactants and Products for ESCM Test 1

Similarly for Test 3, it was found that when the percent total Cl atoms not tied to the alkali metals that exist as either Cl atom or Cl_2 was set at 20%, and the percent approach to the equilibrium Cl_2/Cl ratio set at 0.22%, then the initial concentrations of Cl and Cl_2 would be 6.09×10^{-10} and 4.33×10^{-10} mole/cm^3, respectively. As expected, the resulting initial concentration of Cl for Test 3 was calculated to be lower than that for Test 1, while the resulting initial concentration of Cl_2 was higher than its counterpart for Test 1, since the temperature was lower during Test 3. It is interesting to note that the calculated percent total Cl atoms not tied to the alkali metals that exist as either Cl atom or Cl_2 increased from 13.5 to 20%, as the temperature was decreased from Test 1 to Test 3. This is due to the fact that the formation of Cl_2 is favored over that of Cl atom at lower temperatures, and the net effect is to increase the number of total Cl atoms in both Cl and Cl_2.

Figure 4-2 shows that the calculated $HgCl/HgCl_2$ ratio would match the experimental value of 1 at these initial concentrations of Cl and Cl_2. Due to a lower temperature, it took about three times as long to complete the chlorination reactions as in Test 1. However, the reactions were still complete in 0.15 ms, which is four orders of magnitude shorter than the estimated gas residence time of 14 seconds for Test 3. This confirms the earlier conclusion that the chlorination of mercury will be complete at the instant Cl and Cl_2 are formed. The model also predicted that at the Cl/Hg ratio of 12, 85% of the mercury fed was chlorinated either to HgCl or $HgCl_2$ in both ESCM tests.

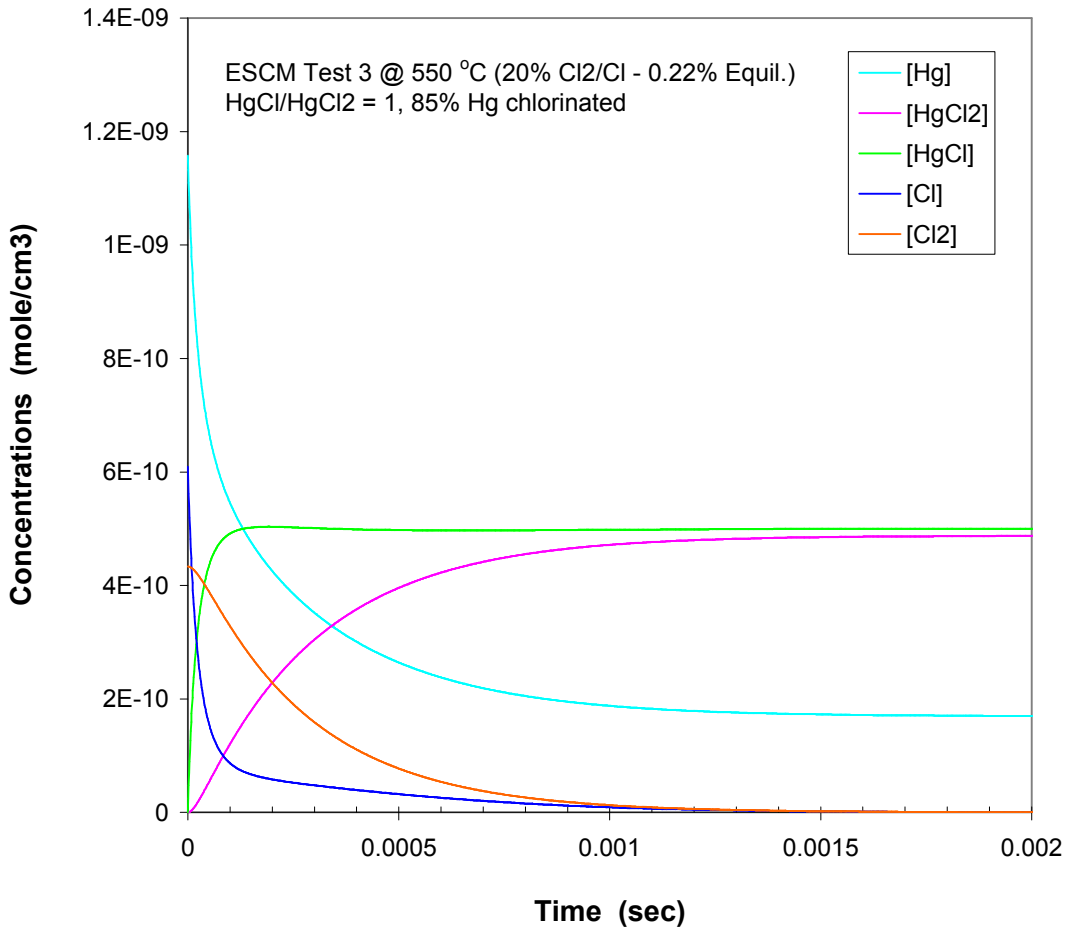

Figure 4-2 Concentration Profiles of Mercury Chlorination Reactants and Products for ESCM Test 3.

The equilibrium model also predicted that practically all NaCl and $LiBO_2$ vapors would condense at 650 °C gas temperature, and all CsCl vapor would condense as well by 450 °C. It means that these semi-volatile salts would form sub-micron sized aerosols before they reach the quencher. The compositions of the melter exhausts after the chlorination reactions are shown in Table 4-3 under the heading EQUIL+KINETIC.

4.2 MODELING OF DWPF

The goal of the ESCM modeling in Section 4.1 was to determine: (1) the percent total Cl atoms not tied to the alkali metals that exist as either Cl atom or Cl_2, and (2) the percent approach to the equilibrium Cl_2/Cl ratio at different temperatures. Now, with the values of these critical parameters determined at 650 and 450 °C actual gas temperatures, the same Zone 1 and 2 models can be run under DWPF conditions. The particular operating scenario that was simulated in this study was Sludge Batch 5 (SB5) simulant composition with no mercury removal during the Chemical Processing Cell (CPC) operations.

4.2.1 DWPF Zone 1 Model

The composition of the SB5 melter feed with no mercury removal is shown in Table 4-4. The feed rate of HgO was set by applying the Hg-to-Fe mass ratio of 0.1448 used in the SB5-C simulant.[2] Given component feed rates are based on the DWPF design basis glass production rate of 228 lb/hr but at 38% waste loading (Frit 510 made up the remaining 62%), 130% stoichiometric acid addition, and 45% total solids. The molar Cl-to-Hg ratio is only 0.4, compared to 12 for the ESCM feeds, which means that there is a significant deficit in chloride so the overall conversion of elemental mercury into HgCl and/or $HgCl_2$ is expected to be very low.

The results of the FactSage model run at 1,150 ^{o}C are shown in Table 4-5. As expected, 100% of the mercury fed as HgO was predicted to volatilize as elemental mercury vapor. At 1,150 ^{o}C under equilibrium conditions, 100% of the chloride fed was also predicted to volatilize as either HCl or alkali chlorides at a ratio of 25:75, respectively. Notice that the percent total Cl atoms that couple with alkali metals was predicted to be much higher than for the ESCM feeds. Perhaps due to a significant shortage of chloride atoms, neither Cl atoms nor Cl_2 were predicted to form at any concentrations. As with the ESCM results, these model predictions do not include any physically-entrained solids.

The measured redox of the SB5 feed with a nominal mercury content was 0.25 (Fe^{2+}/total Fe in the glass).[2] So, the redox with zero percent mercury removal is expected to be <0.25, since one oxygen atom is released for each elemental mercury released. As with the ESCM feeds, however, the predicted melt composition of the SB5 simulant appears to be severely reducing, as evidenced by the formation of FeO and sulfides such as Ni_3S_2 (Table 4-5). Again, this is likely the result of the single-stage cold cap modeling. The reducing nature of the SB5 glass does not impact the volatilization of mercury and chloride, so it has no impact on this study. It is interesting to note that the FactSage single-stage model predicted the formation of nepheline ($NaAlSiO_4$) as part of the non-stoichiometric condensed phase.

Table 4-4 Composition of DWPF SB5 Melter Feed with No Hg Removal.

Insoluble Solids	lb/hr	mole/hr	Soluble Solids	lb/hr	mole/hr
FeOOH	2.9086E+01	1.4849E+02	Ca(COOH)2	2.8930E+00	1.0088E+01
Al(OH)3	1.8611E+01	1.0822E+02	Ca(NO3)2	0	0
MnO2	6.7067E-01	3.4991E+00	Co(COOH)2	0	0
Ca(OH)2	9.6045E-01	5.8797E+00	Co(NO3)2	0	0
Na2U2O7	0	0	CsCOOH	0	0
Mg(OH)2	1.6025E+00	1.2466E+01	CsNO3	0	0
HgO	2.8585E+00	5.9864E+00	Cu(COOH)2	4.8833E-03	1.4426E-02
Ca3(PO4)2	5.1982E-01	7.6017E-01	Cu(NO3)2	0	0
Ni(OH)2	2.6321E+00	1.2879E+01	KCOOH	0	0
Cr(OH)3	3.3888E-02	1.4921E-01	KNO3	3.6052E-01	1.6175E+00
Cu(OH)2	1.2409E-02	5.7704E-02	Mg(COOH)2	7.8531E-01	3.1165E+00
TiO2	8.9136E-03	5.0603E-02	Mg(NO3)2	0	0
SiO2	1.0127E+02	7.6446E+02	Mn(COOH)2	1.0063E+01	3.1492E+01
Na2O	1.1309E+01	8.2763E+01	Mn(NO3)2	0	0
ThO2	0	0	NH4COOH	0	0
Zn(OH)2	8.8154E-03	4.0236E-02	NH4NO3	0	0
PuO2	6.6135E-03	1.1074E-02	NaCl	3.0156E-01	2.3405E+00
K2O	0	0	NaF	0	0
RuO2	2.5245E-02	8.6052E-02	NaCOOH	3.2183E+01	2.1468E+02
RhO2	2.7373E-02	9.2036E-02	NaNO3	1.7714E+01	9.4533E+01
PdO	9.6319E-04	3.5695E-03	NaNO2	0	0
Ce(OH)3	1.7604E-02	4.1775E-02	Na3PO4	0	0
SrCO3	0	0	Ni(COOH)2	1.0556E+00	3.2198E+00
B2O3	1.9790E+01	1.2894E+02	Ni(NO3)2	0	0
Li2O	1.1309E+01	1.7166E+02	Pb(NO3)2	0	0
Cs2O	0	0	Pd(NO3)2	0	0
BaSO4	2.2931E-02	4.4567E-02	Sr(COOH)2	0	0
Gd(OH)3	0	0	Sr(NO3)2	0	0
PbSO4	0	0	UO2(COOH)2	4.6770E+00	5.8920E+00
TcO2	0	0	UO2(NO3)2	0	0
La(OH)3	1.0561E-02	2.5222E-02	La(COOH)3	3.8083E-03	6.3055E-03
ZrO2	0	0	La(NO3)3	0	0
CaCO3	0	0	Zn(COOH)2	3.4457E-03	1.0059E-02
CaSO4	5.7859E-01	1.9278E+00	Zn(NO3)2	0	0
CaC2O4	0	0	Na2CO3	0	0
Na2C2O4	0	0	Na2C2O4	0	0
AlOOH	9.5415E+00	7.2146E+01	Na2SO4	6.5880E-02	2.1039E-01
MgO	0	0	HCOOH	1.1912E+00	1.1747E+01
Coal	1.4916E-01	5.6384E+00	Isopar L	7.3681E-03	2.3490E-02
Total Insoluble	2.1106E+02	1.5263E+03	Total Soluble	7.1310E+01	3.7899E+02
			H2O	3.4246E+02	8.6228E+03
			Total Slurry	6.2483E+02	1.0528E+04
			molar Cl/Hg =		0.39

Table 4-5 FactSage Equilibrium Model Results at 1,150 ^{o}C for DWPF SB5 Run.

PHASE: gas_ideal	mole/hr	PHASE: BSlag-liq	mole/hr
H2O	4.6241E+02	MgO	1.5582E+01
CO2	3.2080E+02	MnO	3.4991E+01
N2	4.8075E+01	Na2O	1.7346E+02
CO	1.8876E+01	SiO2	4.5386E+02
H2	1.2187E+01	CaO	1.7895E+01
Hg	5.9862E+00	Al2O3	6.6515E+01
UO3	4.9525E+00	K2O	8.0203E-01
SO2	1.9327E+00	NiO	2.1672E+00
NaCl	1.1821E+00	Fe2O3	6.2831E-01
UO3(H2O)	9.3842E-01	B2O3	4.1966E+01
LiBO2	8.8552E-01	MnSO4	3.4962E-05
HBO2	6.6122E-01	NiSO4	2.1653E-06
NaBO2	6.2864E-01	Fe2(SO4)3	6.2779E-07
HCl	5.7867E-01	Na2SO4	1.7332E-04
LiCl	5.5102E-01	K2SO4	8.0136E-07
H3BO3	3.1768E-01	CaSO4	1.7881E-05
H2S	8.6832E-02	MgSO4	1.5569E-05
LiOH	4.9579E-02	TOTAL:	8.0787E+02
NaOH	1.7826E-02		
Fe(OH)2	9.1785E-03	PHASE: Non-stoichiometric	mole/hr
(NaCl)2	8.9275E-03	NaAlSiO4	4.7336E+01
KBO2	8.9091E-03	Si2O4	5.7443E+00
SO	7.5636E-03	TOTAL:	5.3080E+01
KCl	4.4900E-03		
COS	4.4188E-03	PHASE: pure liquids	mole/hr
Na	2.7477E-03	Li2Si2O5 (liq)	1.2589E+02
(LiCl)2	1.8446E-03	LiBO2 (liq)	9.0059E+01
HS	1.5986E-03	NaBO2 (liq)	8.1386E+01
S2	1.4821E-03	FeO (liq)	6.9869E+01
(HBO2)3	1.3307E-03	Fe3O4 (liq)	2.5784E+01
Ni(OH)2	7.3026E-04	Ni (liq)	1.3779E+01
UO2Cl2	7.0538E-04	Ni3S2 (liq)	5.0774E-02
H	6.8437E-04	TOTAL:	4.0682E+02
OH	5.7937E-04		
FeCl2	5.0267E-04		
TOTAL:	8.8117E+02		

4.2.2 DWPF Zone 2 Model

As with the ESCM case, the DWPF Zone 2 model consisted of two parts. The first was the FactSage model to calculate the equilibrium compositions of the melter exhausts at the measured melter vapor space temperatures of 650 ^{o}C. The second part was the gas-phase kinetics model of mercury chlorination which further adjusted the equilibrium speciation of mercury. The input for the Zone 2 FactSage model included:

(1) the ideal-gas output shown in Table 4-5,
(2) free H_2O that volatilizes from the cold cap,
(3) the melter air inleakage and purge.

The flow rate of free H_2O is given in Table 4-4 and the rates of melter air inleakage and backup film cooler purge were set at 50 and 370 lb/hr, respectively.

The results of the Zone 2 FactSage model runs for SB5 simulant are shown in Table 4-6 under the heading EQUIL. One notable result is that the percent total Cl atoms predicted to exist as alkali chlorides decreased from 75% of the total chloride fed at 1,150 °C to zero as the melter exhaust was cooled below 850 °C. By contrast, the percent total Cl atoms predicted to exist as alkali chlorides were 35-40% even at lower temperatures for the ESCM feeds. The summary of gas-phase results also shows that equilibrium favors: (1) nearly 65% of the total chloride fed to oxidize the mercury, (2) much of the remaining 35% to be in the form of HCl, and (3) the formation of Cl_2 over Cl at 550 °C actual gas temperature at a ratio of nearly 6:1.

Since the nominal DWPF melter vapor space temperature was right at the midpoint of the two ESCM temperatures, the percent total Cl atoms not tied to the alkali metals that exist either as Cl atom or Cl_2 was set at 16.75%, which is the average of the two corresponding ESCM values. Likewise, the percent approach to the equilibrium Cl_2/Cl ratio was set at 0.61%, which is again the average of the two corresponding ESCM values. The resulting initial concentrations of Cl and Cl_2 for the DWPF SB5 feed were 3.67×10^{-10} and 6.53×10^{-12} mole/cm^3, respectively (Table 4-6). At these initial concentrations of Cl and Cl_2, the calculated HgCl/$HgCl_2$ ratio was 53, which means that >98% of the chlorinated mercury would have an oxidation state of +1. It is also noted that with so few Cl atoms available compared to Hg, the reactions are essentially complete in 0.03 ms, and only 6% of the mercury fed would be chlorinated. As shown in Table 4-6, the remaining 94% of the mercury fed would exist as either Hg^0 (90%) or HgO (4%).

It is noted that the measured chloride level in the SB5 qualification sample was an order of magnitude lower than that of the SB5 simulant used in this study. As a result, the degree of shortage in chloride in relation to mercury will be even greater in the actual SB5 feed. This would make the predicted level of HgCl in the actual SB5 melter exhaust lower than 6% of the total mercury fed, while that of elemental mercury is expected to be greater than 90%. This means that much of the mercury fed will likely condense as the elemental mercury in the Quencher.

Table 4-6 Results of Zone 2 FactSage and Kinetic Model Runs for DWPF SB5.

DWPF Run	SB5+100% Hg	SB5+100% Hg
Calculation Mode	EQUIL	EQUIL+KINETIC
Measured Melter VS T (°C)	650	650
Melter VS Gas T (°C)	550	550
PHASE: gas_ideal	mole/hr	mole/hr
H2O	9.0954E+03	9.0954E+03
N2	4.6201E+03	4.6201E+03
O2	1.1981E+03	1.1981E+03
CO2	3.3968E+02	3.3968E+02
Hg	4.9958E+00	5.3754E+00
H3BO3	2.4985E+00	2.4985E+00
HCl	8.1161E-01	1.9463E+00
HgCl2	7.6308E-01	7.0938E-03
SO3	3.0045E-01	3.0045E-01
HgO	2.2726E-01	2.2726E-01
SO2	4.6700E-02	4.6700E-02
NO	1.9651E-02	1.9651E-02
O2S(OH)2	8.1518E-03	8.1518E-03
NO2	2.8861E-03	2.8861E-03
(HBO2)3	1.1539E-03	1.1539E-03
OH	5.2687E-05	5.2687E-05
HBO2	4.1111E-05	4.1111E-05
Cl2	3.1736E-05	4.8675E-04
HOCl	2.4305E-05	2.4305E-05
Cl	1.0883E-05	6.6001E-06
Hg2	6.1875E-06	6.1875E-06
HgCl	7.3251E-07	3.7643E-01
KCl	6.7573E-07	6.7573E-07
NaCl	3.6186E-07	3.6186E-07
TOTAL:	1.5263E+04	1.5264E+04
PHASE: condensed	mole/hr	mole/hr
UO3 (s)	5.8909E+00	5.8909E+00
LiNa(SO4) (s)	1.4764E+00	1.4764E+00
Na2SO4 (s)	1.8640E-01	1.8640E-01
KLi(SO4) (s)	1.3398E-02	1.3398E-02
Fe2O3 (s)	4.5892E-03	4.5892E-03
TOTAL:	7.5717E+00	7.5717E+00
Summary of Gas-Phase Results		
% Cl tied to alkali metals	0.00	0.00
% Cl not tied to alkali metals	100.00	100.00
% Cl as Cl-Cl2 in non-alkali Cl	0.00	16.75
% approach to equilibrium	-	0.61
ratio Cl as Cl2/Cl atom	5.83	0.04
initial conc [Cl]o (mole/cm3)	1.0558E-14	3.6686E-10
initial conc [Cl2]o (mole/cm3)	3.0789E-14	6.5258E-12
calculated HgCl/HgCl2	0.00	53.06
Chlorinated Hg (% total Hg)	12.75	6.41

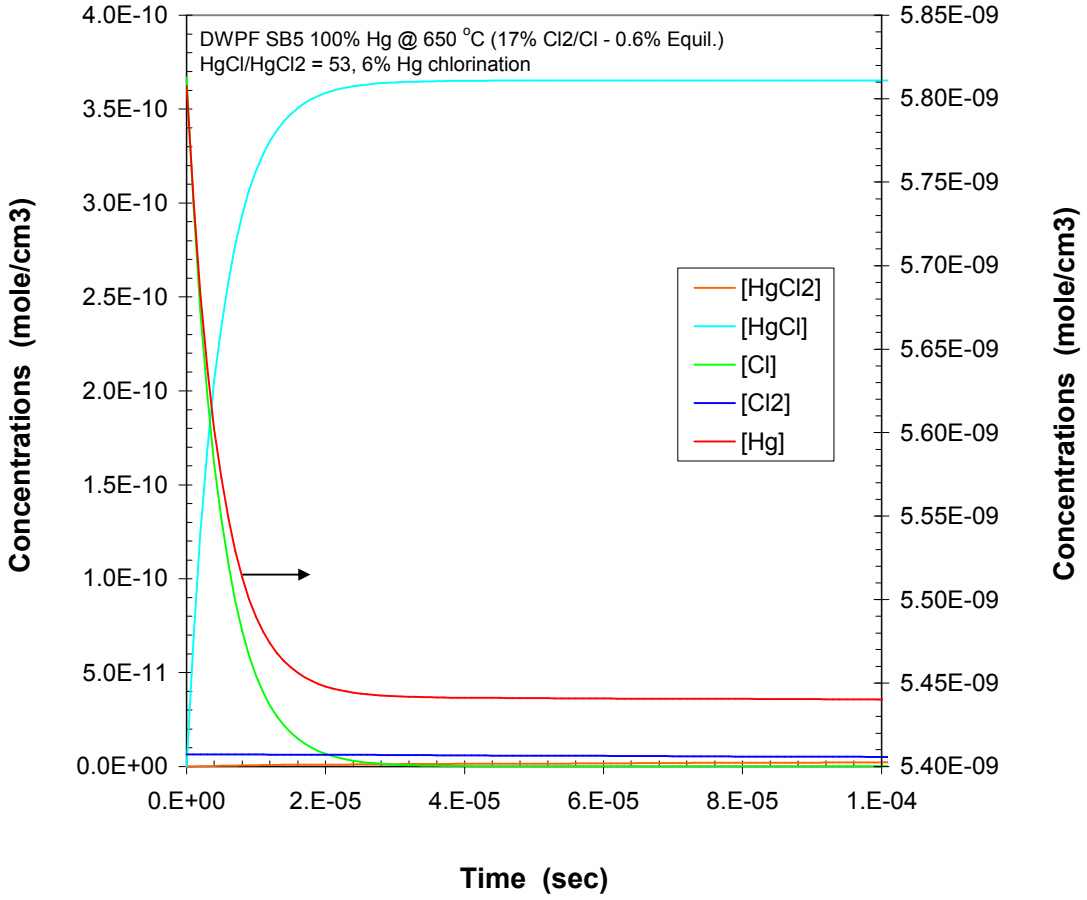

Figure 4-3. Concentration Profiles of Mercury Chlorination Reactants and Products for DWPF SB5 Feed with Zero Mercury Removal in CPC.

4.3 COMBINED HOMOGENEOUS GAS PHASE AND LIQUID PHASE OXIDATION – ESCM TESTS

The homogeneous oxidation results from the FactSage modeling in Section 4.1 for Tests 1 and 3 were used as inputs to an approximate liquid-phase model. This composition did not contain any entrained glass or feed. For the results from both tests, the offgas composition was cooled to 25 °C, resulting in aqueous condensate, a gas phase, and precipitated Hg species. Because of the effect of O_2 on the redox of mercury, the O_2 in these streams was converted mole-for-mole to inert N_2. The OLI model input species are shown in Table 4-7. Species specific to FactSage that are not valid species in OLI were adjusted as shown. For the OLI input, the phase does not matter, so the gas phase and condensed phase species were added.

Table 4-7 FactSage Output and Input to OLI Aqueous Model

	ESCM Test 1 FactSage Equil+Kinetic	OLI Input Adjusted	ESCM Test 3 FactSage Equil+Kinetic	OLI Input Adjusted
Vapor	mol/h	mol/h	mol/h	mol/h
H_2O	1.52E+02	1.52E+02	5.44E+01	5.44E+01
N_2	2.00E+01	2.52E+01	1.99E+01	2.52E+01
O_2	5.12E+00	0	5.22E+00	0
CO_2	2.20E+00	2.20E+00	8.18E-01	8.18E-01
HCl	9.47E-02	9.47E-02	2.82E-02	2.82E-02
HF	4.47E-02	4.47E-02	0.00E+00	0.00E+00
H_3BO_3	3.81E-02	3.81E-02	1.70E-02	1.70E-02
CsCl	7.82E-03	1.06E-02	1.18E-05	3.82E-03
Hg	1.83E-03	1.83E-03	8.08E-04	8.08E-04
HgCl	1.20E-02	1.20E-02	2.39E-03	2.39E-03
$HgCl_2$	1.37E-03	1.37E-03	2.33E-03	2.33E-03
HgO	2.70E-04	2.70E-04	4.18E-07	4.18E-07
Hg(I)	%	77.6	%	43.2
Hg(II)		10.6		42.2
Hg(0)		11.8		14.6
$(CsCl)_2$	1.41E-03	CsCl above	4.04E-06	CsCl above
NaCl	1.23E-03	6.17E-02	1.95E-07	2.67E-02
LiCl	8.96E-04	1.37E-03	2.49E-07	3.74E-07
$(NaCl)_2$	3.95E-04	NaCl above	2.94E-08	NaCl above
NO	3.54E-04	3.54E-04	1.37E-05	1.37E-05
$(LiCl)_2$	2.38E-04	LiCl above	6.28E-08	LiCl above
NO_2	1.24E-05	1.24E-05	5.98E-06	5.98E-06
$(HBO2)_3$	1.32E-05	none	9.55E-06	none
Cl_2	5.76E-07	2.13E-06	3.23E-11	4.81E-11
OH	7.46E-06	none	1.07E-08	none
Cl	3.11E-06	Cl_2 above	3.15E-11	Cl_2 above
Condensed				
NaCl	5.97E-02	NaCl above	2.67E-02	NaCl above
$LiNaSO_4$	1.65E-02	$Li_2SO_4 + Na_2SO_4$	1.53E-03	$Li_2SO_4 + Na_2SO_4$
Na_2SO_4	none	8.27E-03	none	7.67E-04
$LiBO_2$	9.85E-03	9.85E-03	0.00E+00	0.00E+00
Li_2SO_4	6.52E-03	1.48E-02	6.78E-03	7.54E-03
CsCl	0.00E+00	CsCl above	3.80E-03	CsCl above

The pH of the DWPF condensate sample was approximately 2.5, so the pH was adjusted to this value in the aqueous models by adding NaOH. The pH without adjustment was about 1.6. The temperature and pressure were assumed to be 25 °C and 1 atm. Ambient temperature was chosen because even though the condensate tank temperature was higher, the samples were cooled to room temperature before analysis, so the actual speciation measured would be that at room temperature.

The target ratios of the mercury species are shown in the first column of Table 4-8. The FactSage output is shown in the second column. The third column shows the OLI model output using the inputs from Table 4-7. For both tests, the amount of Hg(I) is over-

predicted. Because the proportion of chlorine present as Cl_2 at the quench temperature of around 45-60 °C will be higher than those in Table 4-7 (at 650 and 450 °C), the amount of Cl_2 was adjusted in the OLI model. The predicted mercury speciation for the best Cl_2 amount and the same amount for each test is shown in columns 4-5 of Table 4-8. The original and adjusted amounts of Cl_2 are shown in the bottom two rows. For both cases, increasing the Cl_2 amount to around 7.45×10^{-4} mol gives mercury speciation that matches the target values.

Table 4-8 Product Percentages for ESCM Test Model

	Hg_2^{2+} : Hg^{2+} : Hg^0				
ESCM Test	**Condensate Target**	**FactSage Output and OLI Input**	**OLI Predicted, No Cl_2 Adjustment**	**OLI Predicted, each Test's Cl_2 Adjusted Individually**	**OLI Predicted, Cl_2 Adjusted to Same for Both Tests**
1	90 : 10 : ~0	77 : 11 : 12	99 : 0 : 1	90 : 10 : 0	92 : 8 : 0
3	50 : 50 : ~0	43 : 42 : 15	73 : 27 : 0	50 : 50 : 0	46 : 54 : 0
1	Cl_2 Amount (mol):		2.13E-06	8.7E-04	7.45E-04
3	Cl_2 Amount (mol):		4.81E-11	6.2E-04	7.45E-04

In future work, the FactSage model will be used to predict the actual amount of chlorine present at the quencher inlet temperature.

5.0 CONCLUSIONS

Based on an extensive review of the literature data on mercury chemistry, the speciation of mercury in the DWPF melter off-gas system was modeled in three stages in this work. In the first stage, the calcination and fusion of the melter feed in the cold cap and melt was modeled using thermodynamic equilibrium software called FactSage. The FactSage equilibrium model predicted that 100% of the mercury and chloride fed would volatilize as elemental mercury and alkali salts/HCl, respectively, at 1,150 ^{o}C. The composition of the calcine gases thus calculated was re-equilibrated along with the air inleakage and the free H_2O of the slurry feed in the second stage at the melter vapor space gas temperature. The mercury and those chloride species that are not tied to the alkali metals, as predicted by the second-stage FactSage model, were allowed to undergo a set of homogeneous gas-phase oxidation reactions in the third stage.

The gas-phase oxidation kinetics model contains two critical parameters pertaining to the partitioning of non-alkali-metal-bound chloride atoms among HCl, Cl, and Cl_2. In other words, the equilibrium-predicted partitioning of HCl/Cl/Cl_2 at the melter vapor space gas temperature was re-adjusted prior to the oxidation reactions of the third stage in order to account for the effect of non-equilibrium on the gas-phase speciation of chloride. The values of these model parameters were determined at two different melter vapor space temperatures by matching the predicted molar ratio of HgCl to $HgCl_2$ with those measured during the ESCM tests. The calibrated model was then run with the DWPF SB5 simulant under the hypothetical operating scenario of zero mercury removal in the CPC, resulting in a Cl-to-Hg molar ratio of only 0.4 in the melter feed. The results of the model run at 650 ^{o}C indicated melter vapor space temperature (TI4085D) showed that due to excessive shortage of chloride, only 6% of the mercury fed is expected to get oxidized, mostly as HgCl, while the remaining would exist either as elemental mercury (90%) or HgO (4%). Since the SB5 simulant composition used in this work had an order of magnitude higher chloride level than those measured for the SB5 qualification samples, the degree of chloride shortage would be even more pronounced in the actual SB5 feed, and the likely conversion of mercury chlorination is expected to be even lower than 6%. This means that over 90% of the mercury fed would likely enter the quencher as elemental mercury vapor.

The homogeneous oxidation of mercury in the off-gas was deemed to be of primary importance for the formation of sub-micron sized aerosols upon condensation. It is these semi-volatiles that can deposit in the off-gas lines downstream of the OGCT. Formation of these sub-micron semi-volatile salts in the condensate liquid was considered to be unlikely, so the liquid phase reactions were considered to be less important. Furthermore, it should be noted that all model predictions presented in this report represent the vapor pressure driven off-gas carryover, and any physically-entrained solids, which typically account for much of the off-gas carryover on a mass basis, were excluded in this work. However, the subsequent oxidation of mercury in the liquid phase in the off-gas system was examined in a simplified model of the off-gas condensate and it was found that the

condensate chemistry was consistent with further oxidation of elemental mercury to Hg_2Cl_2 and conversion of HgO to chlorides.

There are many process benefits to be gained by removing the mercury-stripping step in the CPC. This work was initiated to study what impact zero mercury removal in the CPC would have on the melter off-gas system. It is stressed that this study was intended to be scoping in nature, so the results presented in this report are only preliminary.

6.0 PATH FORWARD

The implementation of the zero-mercury-removal flowsheet in the DWPF would require further substantiation of the results presented in this report through a more in-depth modeling study and subsequent validation of ensuing theoretical predictions with the proof-of-principle experiments. This effort should include compilation and comparison of data from past DWPF operations on the concentrations of chloride, mercury and other relevant species, off-gas system particulate deposition and plugging, off-gas system performance and configuration, and deposit compositions. With much of the mercury fed to the melter expected to be present as elemental mercury vapor at the Quencher inlet, it is essential to look into the mechanism of mercury condensation in the Quencher and further downstream. For instance, it would be of great practical value to find out what factors influence the mode of mercury condensation, i.e., whether it would have a tendency to form droplets or coat available surfaces and, if they form droplets, how mercury droplets would grow in size. In addition, expansion of the current model in terms of both depth and scope would undoubtedly shed additional insight into the speciation of mercury as a function of both feed chemistry and key melter operating variables.

It is proposed that additional efforts be put on the following areas:

- Compile and compare data from past DWPF operations to better understand the potential effects of mercury species on off-gas system performance.
- Expansion of Zone 2 oxidation kinetics model.
- Inclusion of Zone 3 aqueous-phase reactions.
- Mechanism of Cl/Cl_2 formation.
- Mechanisms for mercury condensation and growth of droplets.
- Validation with the proof-of-principle experiments.

7.0 REFERENCES

1. R.W. Goles, G.J. Sevigny, and C.M. Andersen, "LFCM (Liquid-Fed Ceramic Melter) Processing Characteristics of Mercury," Report No. PNL-SA-17928; CONF-900809-5, 1990.

2. D.P. Lambert, M.E. Stone, B.R. Pickenheim, and D.C. Koopman, "Sludge Batch 5 Simulant Flowsheet Studies," Report No. USDOE SRNS-STI-2008-00024, Rev. 0, 2008.

3. B.R. Pickenheim and K.J. Imrich, "Task Technical & QA Plan - Slurry Receipt and Adjustment Tank (SRAT) Alternative Reductant Assessment," Report No. SRNS-RP-2008-00218, Rev. 0, 2008.

4. N.E. Bibler, "Characterization of Three Samples Taken from the Off Gas System of DWPF Melter One," Report No. USDOE WSRC-TR-2003-00423, 2003.

5. K. Zeigler and N. Ned Bibler, "Characterization of DWPF Melter Off-Gas Quencher and Steam Atomized Scrubber Deposit Samples," Report No. USDOE WSRC-STI-2007-00262, 2007.

6. T.L. Fellinger, "Results for the DWPF Slurry Mix Evaporator Condensate Tank, Off Gas Condensate Tank, and Recycle Collection Tank Samples," Report No. USDOE WSRC-TR-2004-00577, 2004.

7. M.S. Hay and T.L. Fellinger, "Characterization and Dissolution Test Results for the January 2005 DWPF Off Gas Condensate Tank Samples," Report No. USDOE WSRC-TR-2005-00141, 2005.

8. R.D. Eddy and A.W.C. Menzies, "The Solubilities of Certain Inorganic Compounds in Ordinary Water and in Deuterium Water," *The Journal of Physical Chemistry,* **44** [2] 207-35 (1940).

9. H.L. Clever, S.A. Johnson, and M.E. Derrick, "The Solubility of Mercury and Some Sparingly Soluble Mercury Salts in Water and Aqueous-Electrolyte Solutions," *J. Phys. Chem. Ref. Data,* **14** [3] 631-81 (1985).

10. L.G. Hepler and G. Olofsson, "Mercury - Thermodynamic Properties, Chemical-Equilibria, and Standard Potentials," *Chem. Rev.,* **75** [5] 585-602 (1975).

11. O.S. Pokrovsky, "Experimental-Determination of the Association Constant of Mercurous Ion with Chloride in Aqueous-Solutions at 20-80 °C," *Geokhimiya,* [6] 881-94 (1995).

12. N.D. Hutson, J.R. Zamecnik, M.E. Smith, D.H. Miller, and J.A. Ritter, "Integrated DWPF Melter System (IDMS) Campaign Report - Mercury Operation," Report No. USDOE WSRC-TR-91-0363, 1991.

13. J.R. Zamecnik, "Measurement of Cesium and Mercury Emissions from the Vitrification of Simulated High Level Radioactive Waste," Report No. USDOE WSRC-MS-92-268; CONF-930906-1, 1992.

14. B.J. Aylett, "Mercury," in *Comprehensive Inorganic Chemistry*. Edited by J. C. Bailar. Pergamon Press, Oxford, U.K., 1973.

15. D. Laudal, B. Nott, T. Brown, and R. Roberson, "Mercury Speciation Methods for Utility Flue Gas," *Fresenius. J. Anal. Chem.,* **358** [3] 397-400 (1997).

16. R.N. Sliger, J.C. Kramlich, and N.M. Marinov, "Towards the Development of a Chemical Kinetic Model for the Homogeneous Oxidation of Mercury by Chlorine Species," *Fuel Processing Technology,* **65-66** 423-38 (2000).

17. M.H. Mendelsohn and C.D. Livengood, "Critical Review of Mercury Chemistry in Flue Gas," Report No. USDOE ANL/ESD/06-4, 2006.

18. P.H. Taylor, R. Mallipeddi, and T. Yamada, "LP/LIF Study of the Formation and Consumption of Mercury(I) Chloride: Kinetics of Mercury Chlorination," *Chemosphere,* **61** [5] 685-92 (2005).

19. B. Hall, P. Schager, and O. Lindqvist, "Chemical-Reactions of Mercury in Combustion Flue-Gases," *Water Air Soil Pollut.,* **56** 3-14 (1991).

20. D.G. Horne, R. Gosavi, and O.P. Strausz, "Reactions of Metal Atoms. I. The Combination of Mercury and Chlorine Atoms and the Dimerization of HgCl," *The Journal of Chemical Physics,* **48** [10] 4758-64 (1968).

21. M.H. Xu, Y. Qiao, C.G. Zheng, L.C. Li, and J. Liu, "Modeling of Homogeneous Mercury Speciation Using Detailed Chemical Kinetics," *Combust. Flame,* **132** [1-2] 208-18 (2003).

22. C.L. Senior, A.F. Sarofim, T. Zeng, J.J. Helble, and R. Mamani-Paco, "Gas-Phase Transformations of Mercury in Coal-Fired Power Plants," *Fuel Processing Technology,* **63** [2-3] 197-213 (2000).

23. J.R. Edwards, R.K. Srivastava, and J.D. Kilgroe, "A Study of Gas-Phase Mercury Speciation Using Detailed Chemical Kinetics," *J. Air Waste Manage. Assoc.,* **51** [6] 869-77 (2001).

24. S. Niksa, J.J. Helble, and N. Fujiwara, "Kinetic Modeling of Homogeneous Mercury Oxidation: The Importance of NO and H_2O in Predicting Oxidation in Coal-Derived Systems," *Environ. Sci. Technol.,* **35** [18] 3701-6 (2001).

25. A. Fry, B. Cauch, G.D. Silcox, J.S. Lighty, and C.L. Senior, "Experimental Evaluation of the Effects of Quench Rate and Quartz Surface Area on Homogeneous Mercury Oxidation," *Proceedings of the Combustion Institute,* **31** 2855-61 (2007).

26. K.C. Galbreath, C.J. Zygarlicke, E.S. Olson, J.H. Pavlish, and D.L. Toman, "Evaluating Mercury Transformation Mechanisms in a Laboratory - Scale Combustion System," *Sci. Total Environ.,* **261** [1-3] 149-55 (2000).

27. B. Hall, P. Schager, and J. Weesmaa, "The Homogeneous Gas-Phase Reaction of Mercury with Oxygen, and the Corresponding Heterogeneous Reactions in the Presence of Activated Carbon and Fly-Ash," *Chemosphere,* **30** [4] 611-27 (1995).

28. B. Hall, O. Lindqvist, and E. Ljungstrom, "Mercury Chemistry in Simulated Flue-Gases Related to Waste Incineration Conditions," *Environ. Sci. Technol.,* **24** [1] 108-11 (1990).

29. G.A. Norton, H.Q. Yang, R.C. Brown, D.L. Laudal, G.E. Dunham, and J. Erjavec, "Heterogeneous Oxidation of Mercury in Simulated Post Combustion Conditions," *Fuel,* **82** [2] 107-16 (2003).

30. K. Schofield, "Mercury Emission Chemistry: The Similarities or Are They Generalities of Mercury and Alkali Combustion Deposition Processes?," *Proceedings of the Combustion Institute,* **30** [1] 1263-71 (2005).

31. K. Schofield, "New Method to Minimize High-Temperature Corrosion Resulting from Alkali Sulfate and Chloride Deposition in Combustion Systems. II. Molybdenum Salts," *Energy Fuels,* **19** [5] 1898-905 (2005).

32. K. Schofield, "Let Them Eat Fish: Hold the Mercury," *Chemical Physics Letters,* **386** [1-3] 65-9 (2004).

33. P.A. Ariya, A. Khalizov, and A. Gidas, "Reactions of Gaseous Mercury with Atomic and Molecular Halogens: Kinetics, Product Studies, and Atmospheric Implications," *The Journal of Physical Chemistry A,* **106** [32] 7310-20 (2002).

34. C.J. Lin and S.O. Pehkonen, "The Chemistry of Atmospheric Mercury: A Review," *Atmospheric Environment,* **33** [13] 2067-79 (1999).

35. N.Q. Yan, S.H. Liu, S.G. Chang, and C. Miller, "Method for the Study of Gaseous Oxidants for the Oxidation of Mercury Gas," *Industrial & Engineering Chemistry Research,* **44** [15] 5567-74 (2005).

36. D.L. Laudal, T.D. Brown, and B.R. Nott, "Effects of Flue Gas Constituents on Mercury Speciation," *Fuel Processing Technology,* **65** 157-65 (2000).

37. C.L. Senior, L.E. Bool, G.P. Huffman, and F.E. Huggins, "A Fundamental Investigation of Toxic Substances from Coal Combustion," *Abstr. Pap. Am. Chem. Soc.,* **212** 7-FUEL (1996).

38. S.L. Scott, H. Yusuf, N. Lahoutifard, and K. Maunder (2003). Homogeneous and Heterogeneous Reactions of Atmospheric Mercury(II) with Sulfur(IV), E D P Sciences.

39. "Standard Test Method for Elemental, Oxidized, Particle-Bound and Total Mercury in Flue Gas Generated from Coal-Fired Stationary Sources (Ontario Hydro Method)," ASTM International, ASTM D 6784 - 02, 2008.

40. M.E.A. de Magalhães and M. Tubino, "A Possible Path for Mercury in Biological-Systems - the Oxidation of Metallic Mercury by Molecular-Oxygen in Aqueous-Solutions," *Sci. Total Environ.,* **170** [3] 229-39 (1995).

41. M. Yamamoto, "Stimulation of Elemental Mercury Oxidation in the Presence of Chloride Ion in Aquatic Environments," *Chemosphere,* **32** [6] 1217-24 (1996).

42. M. Amyot, F.M.M. Morel, and P.A. Ariya, "Dark Oxidation of Dissolved and Liquid Elemental Mercury in Aquatic Environments," *Environ. Sci. Technol.,* **39** [1] 110-4 (2005).

43. W.P. Linak, J.V. Ryan, B.S. Ghorishi, and J.O.L. Wendt, "Issues Related to Solution Chemistry in Mercury Sampling Impingers," *J. Air Waste Manage. Assoc.,* **51** [5] 688-98 (2001).

44. B. Cauch, G.D. Silcox, J.S. Lighty, J.O.L. Wendt, A. Fry, and C.L. Senior, "Confounding Effects of Aqueous-Phase Impinger Chemistry on Apparent Oxidation of Mercury in Flue Gases," *Environ. Sci. Technol.,* **42** [7] 2594-9 (2008).

45. L.L. Zhao and G.T. Rochelle, "Mercury Absorption in Aqueous Hypochlorite," *Chem. Eng. Sci.,* **54** [5] 655-62 (1999).

46. L.L. Zhao and G.T. Rochelle, "Mercury Absorption in Aqueous Oxidants Catalyzed by Mercury(II)," *Industrial & Engineering Chemistry Research,* **37** [2] 380-7 (1998).

47. Factsage© Version 6.0, Thermfact/CRCT, Montreal, QC Canada, 2009, www.crct.polymtl.ca.

48. W.P. Colven, "Off-Gas System Data Summary for the Ninth Run of the Large Slurry Fed Melter," Report No. USDOE DPST-83-809, 1983.

49. D.M. Sabatino, J.L. Kessler, and W.P. Colven, "Summary of the Eighth Run of the Large Slurry Fed Melter," Report No. USDOE DPST-83-915, 1983.

50. Solubility Data Series, Vol. 29, *Mercury in Liquids, Compressed Gases, Molten Salts and Other Elements*. Edited by H.L. Clever, M. Iwamoto, S.H. Johnson, and H. Miyamoto. Pergamon Press, Oxford, 1987.

51. Y. Marcus, "Compilation and Evaluation of Solubility Data in the Mercury (U) Chloride-Water System," *J. Phys. Chem. Ref. Data,* **9** [4] 1307-29 (1980).

52. Streamanalyzer 2.0.63, OLI Systems, Inc., Morris Plains, NJ, 2008.

53. *International Critical Tables of Numerical Data, Physics, Chemistry and Technology (1st Electronic Edition)*. Edited by E. W. Washburn. Knovel, (1926 - 1930;2003).

54. J. Sommar, O. Lindqvist, and D. Stromberg, "Distribution Equilibrium of Mercury (II) Chloride between Water and Air Applied to Flue Gas Scrubbing," *J. Air Waste Manage. Assoc.,* **50** [9] 1663-6 (2000).

55. N.D. Hutson, R. Krzyzynska, and R.K. Srivastava, "Simultaneous Removal of SO_2, NO_x, and Hg from Coal Flue Gas Using a $NaClO_2$-Enhanced Wet Scrubber," *Industrial & Engineering Chemistry Research,* **47** [16] 5825-31 (2008).

56. J.C.S. Chang and S.B. Ghorishi, "Simulation and Evaluation of Elemental Mercury Concentration Increase in Flue Gas across a Wet Scrubber," *Environ. Sci. Technol.,* **37** [24] 5763-6 (2003).

57. J.C.S. Chang and Y.X. Zhao, "Pilot Plant Testing of Elemental Mercury Reemission from a Wet Scrubber," *Energy Fuels,* **22** [1] 338-42 (2008).

58. Y.X. Zhao, M.D. Mann, E.S. Olson, J.H. Pavlish, and G.E. Dunham, "Effects of Sulfur Dioxide and Nitric Oxide on Mercury Oxidation and Reduction under Homogeneous Conditions," *J. Air Waste Manage. Assoc.,* **56** [5] 628-35 (2006).

59. A.S. Choi, "Validation of DWPF Melter Off-Gas Combustion Model," Report No. USDOE WSRC-TR-2000-00100, Rev. 0, 2000.

60. T. Co, RK4 Version 3.0 4th-Order Runge-Kutta Solver, Michigan Technological University, Houghton, MI, 2005.